Univerzita Karlova v Praze

Matematicko-fyzikální fakulta

DIPLOMOVÁ PRÁCE

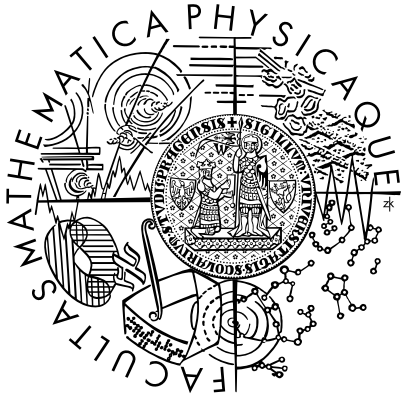

Bc. Martina Zámečníková

Studium biologicky relevantních systémů v elektronicky excitovaných stavech

Katedra chemické fyziky a optiky

Vedoucí diplomové práce: doc. Ing. Pavel Soldán, Dr.

Konzultant: RNDr. Dana Nachtigallová, Ph.D.

Studijní program: Fyzika

Studijní obor: Biofyzika a chemická fyzika

Praha 2014

I thank to my supervisor doc. Ing. Pavel Soldán, Dr. and to my consultant RNDr. Dana Nachtigallová, Ph.D. for interesting topic and stimulating leadership. I also thank to my family and my boyfriend for their never-ending support.

I declare that I carried out this master thesis independently, and only with the cited sources, literature and other professional sources.

I understand that my work relates to the rights and obligations under the Act No. 121/2000 Coll., the Copyright Act, as amended, in particular the fact that the Charles University in Prague has the right to conclude a license agreement on the use of this work as a school work pursuant to Section 60 paragraph 1 of the Copyright Act.

In Prague 11.4.2014 Martina Zámečníková

Název práce: Studium biologicky relevantních systémů v elektronicky excitovaných stavech

Autor: Martina Zámečníková

Katedra: Katedra chemické fyziky a optiky

Vedoucí diplomové práce: doc. Ing. Pavel Soldán, Dr., KCHFO MFF UK

Konzultant: RNDr. Dana Nachtigallová, Ph.D., UOCHB AV ČR

Abstrakt: Dynamika excitovaných stavů izolovaných bází nukleových kyselin je charakterizována velmi krátkou dobou života, v řádu pikosekund, zajišťující fotostabilitu genetického kódu. V molekule nukleových kyselin spolu báze mohou interagovat pomocí patrových interakcí (v rámci jednoho řetězce) nebo vodíkových vazeb (v rámci sousedních řetězců), což výrazně prodlužuje dobu života excitovaných stavů (v řádu nanosekund).Charakter těchto interakcí není dosud zcela objasněn, předpokládá se, že výrazně závisí na typu excitovaného stavu ($\pi \rightarrow \pi^*$). Cílem práce bylo studovat dynamiku excitovaných stavů dimeru N-methylformamidu v komplexu s molekulami vody v excitovaných stavech $n \rightarrow \pi^*$ charakteru.K tomu byla použita neadiabatická "surface hopping" dynamická studie používající multi-referenční popis k výpočtu hyperploch potenciální energie a neadiabatických spřažení. Výsledky ukazují, že ve vertikální oblasti delokalizovaná excitace v S_2 stavu se během několika desítek femtosekund relaxuje do S_1 stavu a lokalizuje na jednom monomeru. Během průběhu dynamiky charakter stavu osciluje mezi lokalizovaným a delokalizovaným. Srovnání s výsledky získanými pro dimery bez přítomnosti vody ukazuje, že hlavním činitelem, který způsobuje delokalizaci, jsou molekuly vody.

Klíčová slova: N-methylformamide dimer, patrové interakce, neadiabatická dynamika, excitované stavy

Title: Study of Biological Systems in Electronically Excited States

Author: Martina Zámečníková

Department: Department of Chemical Physics and Optics

Supervisor: doc. Ing. Pavel Soldán, Dr., KCHFO MFF UK

Consultant: RNDr. Dana Nachtigallová, Ph.D., UOCHB AV ČR

Abstract: Very short lifetimes of excited states of isolated bases in nucleic acids, on the picosecond order, are believed to contribute to photostability of the genetic code. When embedded in DNA this behavior becomes more complex, mainly due to their interactions via stacking and hydrogen bonding. The DNA photophysiscs is not fully understood yet. It depends e.g. on the conformation and the character of excited states. The studies on smaller systems can help to improve the understanding of these phenomena. The aim of this work was to examine the dynamics of the excited states of the $n \rightarrow \pi^*$ character of the complex of N-methylformamide dimer and two waters. The study was performed using non-adiabatic dynamics simulations with on-the-fly Surface Hopping algorithm based on the potential energy surfaces and non-adiabatic couplings obtained with multi-reference approach. The results show that after the vertical excitation into delocalized S_2 state the system relaxes into S_1 state within several tens femtoseconds. For majority of the population, the character of the state then oscillates between localized and delocalized during the whole course of the dynamics. Comparison with calculations with the waters removed indicates that the delocalization is caused by waters serving as a bridge between the two chromophores.

Keywords: N-methylformamide dimer, stacking interactions, non-adiabatic dynamics, excited states

Contents

Introduction

Electronic excitation processes attract attention in the field of organic chemistry, biologically oriented sciences (including DNA), and material science. In particular, the photochemistry of nucleic acids is an important issue since it is related to questions such as stability of genetic code and its damage by UV light. The well-known example of photodamage is the formation of pyrimidine dimers, the reaction which is forbidden in the electronical ground state but allowed in the excited state. In nucleic acids the UV light is absorbed by nucleobases, which were found to have very short excited state lifetime, on the picosecond or sub-picosecond timescale [13, 68]. The nucleobases arrangements in nucleic acids allow efficient interactions which can result in appearance of various excited state phenomena. These were already demonstrated by several experimental groups [17, 39, 43, 69]. Theoretical and experimental studies [16, 17, 39, 43, 52, 69] discuss both interaction motives, i.e. stacking and hydrogen bonding, with the former being probably more important. In addition to the mutual orientation of nucleobases, the importance of the excited state interactions and the character of the excited state was considered.

Despite the huge endeavor of experimental and theoretical chemists, excited state processes, in particular interactions between the bases in DNA are not fully understood. The computational chemistry provides a necessary tool for understanding of mechanisms of processes experimentally observed during the excitation. Theoretical description of excited states in general is quite difficult task which is computationally very demanding to be described accurately enough. With this respect nucleic acids are still challenging systems due to their size, dynamics behavior and their complex structure. Studies performed on small systems allows for the use of highly accurate methods to reveal many mechanistic aspects of excited states which can be used for explanation of the photochemistry of larger systems.

In the present study, N-methylformamide dimer (MF-dimer) is used to study excited state processes between the two chromophores in stacking mutual orientation. To explore the dynamical behavior of these interactions the non-adiabatic dynamics simulations based on the multi-reference method are used. Throughout the studies, the first two excited states of n, π^* character are monitored.

Chapter 1

Theoretical Background to Excitation Processes

Phenomena observed in photochemistry and photobiology involve the processes which occur in the electronically excited states of molecules. Computational chemistry provides a necessary tool for understanding of such phenomena at the molecular level.

To describe a system quantum mechanically, one needs to solve the Schrödinger equation

$$i\hbar\frac{\partial}{\partial t}\Psi = \hat{H}\Psi \tag{1.0.1}$$

where $\hat{H}$ is the Hamiltonian and Ψ the wavefunction of the system. Stationary states can be found by solving the time-independent Schrödinger equation

$$\hat{H}\Psi = E\Psi \tag{1.0.2}$$

The analytical solution for Equation (1.0.2) is possible only for hydrogen atom and hydrogen-like atoms, like He^+, Li^{2+}, and so on. Thus, several approximations are inevitable if someone proposes solving Equation (1.0.2) for a more complex system. The Hamiltonian for a molecular system can be written as

$$\hat{H}(\mathbf{r},\mathbf{R}) = \hat{T}_n + \hat{H}_e(\mathbf{r},\mathbf{R}) \tag{1.0.3}$$

where $\mathbf{R}$ and $\mathbf{r}$ denotes the nuclear and electronic coordinates, respectively, $\hat{T}_n$ the

nuclear kinetic energy operator, and $\hat{H}_e$ the electronic Hamiltonian which contains the electronic kinetic energy operator and Coulombic interactions.

The Hamiltonian (1.0.3) can be written in the form

$$\hat{H} = \hat{T}_n + \hat{T}_e + \hat{V}_{ee} + \hat{V}_{nn} + \hat{V}_{en} \tag{1.0.4}$$

where $\hat{T}_e$ is the kinetic energy of the electrons, $\hat{V}_{ee}$ the Coulombic repulsion of the electrons, $\hat{V}_{nn}$ the Coulombic repulsion of the nuclei, and $\hat{V}_{en}$ is the Coulombic attraction of the electrons and the nuclei. Because the Hamiltonian (1.0.4) neglects any non-electrostatic interactions, it is called an electrostatic Hamiltonian.

The following sections introduce the approximations relevant to the description of excited state processes.

1.1 Born-Oppenheimer Approximation

The Schrödinger equation (1.0.2) with the electrostatic Hamiltonian (1.0.4) is still complicated and can be easily simplified if we consider that nuclei in a molecule are incomparably heavier than electrons. This allows to decouple the different time-scale motions, which is done in the so-called Born-Oppenheimer (BO) approximation. Fixing the nuclei coordinates keeps their repulsion as a constant. Because a constant has no influence on the solution of the Schrödinger equation (1.0.2), it can be also removed from the Hamiltonian (1.0.4).

$$\hat{H}_{\mathrm{BO}} = \hat{T}_e + \hat{V}_{ee} + \hat{V}_{en} \tag{1.1.1}$$

The Hamiltonian (1.1.1) is the termed electronic Hamiltonian in the BO approximation. Since the repulsion of nuclei is a constant that has no impact on the solution of the Schrödinger equation (1.0.2), it can be neglected at this point. The eigenvalues of $\hat{H}_{\mathrm{BO}}$, termed as Potential Energy Surfaces (PES), are then parametrically dependent on the nuclei coordinates. In other words, nuclear motion is governed by a single potential energy surface which describes the electronic energy of one electronic state with respect to changes in the nuclear geometry. The description of the excited state behavior of the system, however, often leads to the situation, where the single-state treatment is qualitatively incorrect and a new framework must be

developed in terms of more electronic states. Such approach will be introduces in Section 1.6.

1.2 Hartree-Fock Approximation

The Hartree-Fock (HF) approximation forms the basis of other more accurate methods in quantum chemistry. It is a variational method in which the ground state wavefunction Ψ_0 corresponds to the state with the lowest possible energy E_0 of the system. This is expressed in

$$E_0 = \langle \Psi_0 | \hat{H} | \Psi_0 \rangle \tag{1.2.1}$$

where $|\Psi_0\rangle$ is a Slater determinant which is thoroughly explained in Appendix A.1. The index 0 in Equation (1.2.1) indicates the ground state of the system. According to the HF approximation, the Slater determinant $|\Psi_0\rangle$ is composed of spin orbitals χ_i that are the eigenvalues of a one-electron operator $\hat{f}(i)$ called the Fock operator (thoroughly explained in Appendix A.3)

$$\hat{f}(i) = -\frac{1}{2}\Delta_i^2 - \sum_{A=1}^{M} \frac{Z_A}{r_{iA}} + \hat{v}^{HF}(i) \tag{1.2.2}$$

which is expressed in this integro-differential equation

$$\hat{f}(i)\chi(x_i) = \varepsilon\chi(x_i) \tag{1.2.3}$$

termed the HF equation, where i designates the i-th electron and $\hat{v}^{HF}(i)$ the averaged potential that the i-th electron "feels" from the other electrons in the system. Since $\hat{v}^{HF}(i)$ depends on the other spin orbitals (as thoroughly explained in Appendix A.3), an iterative procedure has to solve the HF equation (1.2.3). This procedure is called the Size-Consistend Field (SCF) method. The HF equation (1.2.3) gives the full orthonormal basis set which contains both the occupied and the virtual orbitals. One configuration of these spin orbitals results in the approximate ground state wavefunction $|\Psi_0\rangle$. When a system contains an even number of electrons and its orbitals are energetically enough separated, the HF ground state is a reasonable approximation. However, excited states usually need more precise methods to be de-

scribed properly. Thus, the other Slater determinants normally do not approximate excited state wavefunctions but can be used in linear combinations which better approximate these states. More precise approximations for excited state wavefunctions are discussed in the following subsections.

The HF theory deals with spin orbitals in two ways:

(a) if the spatial orbitals of α and β spins are kept the same regardless of the spin, the method is called Restricted HF (RHF)

(b) if the spatial orbitals of α and β spins are allowed to differ according to the spin, the method is called Unrestricted HF (UHF).

The RHF is generally used for closed-shell ground states. The UHF can approximate open-shell excited states.

The integro-differential equation (1.2.3) can be transformed to a set of algebraic equations that are solved by matrix techniques. The function of a spin orbital in Equation (1.2.3) can be expanded

$$\chi_i = \sum_{\mu=1}^{K} C_{\mu i}\phi_\mu \tag{1.2.4}$$

where ϕ_μ is a basis set. If ϕ_μ are functions of atomic orbitals, expansion (1.2.4) is then termed the Linear Combination of Atomic Orbitals (LCAO), and it is widely used in quantum chemistry. Possibilities of choosing a basis set is thoroughly described in Appendix A.4.

Expansion (1.2.4) is truncated, which entails that the resultant spin orbitals only approximate to the exact solution of the HF equation (1.2.3). Now, if one solves the HF equation, he actually seeks the coefficients $C_{\mu i}$. Inserting the spin orbital (1.2.4) into the HF equations and projecting them onto the subspace spanned by $\phi_1, ..., \phi_K$ leads to the generalized eigenvalue problem. The corresponding matrix form

$$FC = SC\epsilon \tag{1.2.5}$$

is called the *Roothaan equations* for the closed-shell RHF method where F denotes the Fock matrix, C the column of coefficients, S the overlap matrix, and ϵ the

energy value. Analogical equations for the open-shell UHF method are called the *Pople-Nesbet equations*.

1.2.1 Correlation Energy

The HF method has the size-consistency feature, but does not include the correlation energy E_{corr} defined as

$$E_{\text{corr}} = E_{\text{exact}} - E_{\text{HF}} \simeq E_{\text{dyn}} + E_{\text{stat}} \tag{1.2.6}$$

where E_{HF} is the HF energy, and E_{exact} is the exact nonrelativistic energy of the system. The correlation energy (1.2.6) distinguishes two parts of the correlation energy: the dynamical correlation energy E_{dyn} and the static correlation energy E_{stat}. The static correlation results from the fact that low-lying states influence and mix strongly with the ground state, which can be overcome in multiconfigurational methods discussed in Sections 1.3 and 1.4. The dynamical correlation arises from the fact that the movement of electrons in a system is not fully correlated in the HF wavefunction, i.e. the wavefunction does not depend on the r_{ij} although the Coulomb repulsive force is present the whole time. The movement is correlated only for the electrons with parallel spin, which is a consequence of the antisymmetry feature of HF wavefunctions.

As Equation (1.2.6) suggests, the correlation energy is not an equal sum of dynamical and static correlation energies. The reason is that E_{stat} involves some E_{dyn} in the systems with two and more electrons.

Nevertheless, other methods are required in order to cover the full correlation energy. In the following text, only the multi-configurational variant of perturbation theory used in presented study will be outlined.

1.3 Multiconfigurational Self-Consistent Field Theory

As stated in Section 1.2, the HF approximation describes correctly the system for which a one-electronic wavefunction is sufficient. It fails, however, for the systems

where more than one electronic configuration contribute to the total wavefunction. The method which is capable to deal with such situations is the Multiconfigurational Size-Consisent Field (MCSCF) method. In this approach, the total wavefunction $|\Psi_{\mathrm{MCSCF}}\rangle$ is a linear combination of Slater determinants (electronic configutations) or a linear combination of Configuration States Functions (CSF) explained in Appendix A.2

$$|\Psi_{\mathrm{MCSCF}}\rangle = \sum_i c_i |\Psi_i\rangle \tag{1.3.1}$$

In this method, both the configuration mixing coefficients c_i and the expansion coefficients of molecular orbitals $C_{\mu i}$ in expansion (1.2.4) are optimized. To keep this approach computationally feasible, expansion (1.3.1) needs to be truncated. The orbitals are usually divided into three groups: inactive, active and external orbitals. The inactive orbitals are kept doubly occupied and the external orbitals are kept unoccupied during the MCSCF optimization. Excitations are allowed only in the active orbitals which constitute the active space. In the so-called Complete Active Space Size-Consistent Field (CASSCF) approximation, all occupations within the active space are considered. The determination of an appropriate CAS wavefunctions is a crucial step in the CASSCF approach. The procedure starts with occupation numbers 0,1 or 2 in active orbitals. The resultant CASSCF wavefunction has the occupation numbers of the active orbitals from 0 to 2 and they do not have to be integer. Although not every MCSCF method is size-consistent, the CASSCF method has this feature.

The CASSCF method can be extended to the Restricted Active Space (RAS) model which further divides CAS of the active orbitals into three groups which further include a maximum number of holes and electrons, respectively. Because of the restrictions in the RAS, the RASSCF allows a bigger CAS than would be possible in the CASSCF method. Thus, the RASSCF can cover the most important dynamic correlation effects.

Examples for which a multiconfigurational approach is necessary are the ground state of ozone molecule, dissociation processes or symmetry forbidden reactions. Significantly, the MCSCF methods are often important in electronically excited states.

When describing a state, it is often useful to optimize more states at the same time. This procedure is termed the State-Averaged (SA) MCSCF.

1.4 Complete Active Space Perturbation Theory

A strong tool in gaining the dynamical correlation are perturbation theories (PT). A PT is used in the cases where an analytical solution is not known and the Hamiltonian can be expressed as a sum

$$\hat{H} = \hat{H}_0 + \hat{W} \tag{1.4.1}$$

where $\hat{H}_0$ is the part of the Hamiltonian for which the analytical solution can be found and $\hat{W}$ is a weak interaction that perturbs the solution of the $\hat{H}_0$. Further, the wavefunction can be expanded to the form

$$|\Psi_{PT}\rangle = |\Psi^{(0)}\rangle + \lambda|\Psi^{(1)}\rangle + \lambda^2|\Psi^{(2)}\rangle + \cdots \tag{1.4.2}$$

and the energy of the system to the form

$$E = E^{(0)} + \lambda E^{(1)} + \lambda^2 E^{(2)} + \cdots \tag{1.4.3}$$

This procedure is a time-independent PT also called the Rayleigh-Schrödinger PT.

When taking $|\Psi_{\mathrm{MCSCF}}\rangle$ as the zeroth-order wavefunction, it is necessary to use a multiconfigurational perturbation theory, for instance the Complete Active Space Perturbation Theory (CASPT) having $|\Psi_{\mathrm{CASSCF}}\rangle$ as the zeroth-order wavefunction. The most common CASPT method is to the second order, termed CASPT2.

The CASPT2 can be calculated by two different ways resulting in: the Single-state CASPT2 (SS-CASPT2), or the Multi-state CASPT2 (MS-CASPT2). The reference space in SS-CASPT2 is one-dimensional and is spanned by a CASSCF reference state, while in MS-CASPT2 the reference state is multi-dimensional and spanned by two or more SA-CASSCF states. Instead of CASSCF functions, other types of CAS functions that are not explained here are possible. The SS-CASPT2 has problem in avoided-crossing areas and in cases of valence-Rydberg mixing at the

CASSCF level. The MS-CASPT2 solves these weaknesses.

In general, the CASPT2 method underestimates bond energies between 2 and 5 kcal/mol for each formed bond. Every time, when the number of electrons is changed, an error corresponding to each electron pair will occur. This error is systematic, and it influences also calculations of excitation energies in way that they are smaller than in reality. This can be fixed by modifying the zeroth-order Hamiltonian.

So-called IPEA level shift decreases the error considerably. The point is to alter the energy of orbitals excited out to be more IP (ionization potential) like and the energy of orbitals excited into to be more EA (electron affinity) like. This can be obtained by adding terms, simply called shifts,

$$\sigma_p^{EA} = \frac{1}{2} D_{pp} \epsilon \tag{1.4.4}$$

$$\sigma_p^{IP} = -\frac{1}{2}(2 - D_{pp})\epsilon \tag{1.4.5}$$

to the diagonal terms of the Fock matrix

$$F_{pp} = -\frac{1}{2}[D_{pp}(IP)_p + (2 - D_{pp})(EA)_p] \tag{1.4.6}$$

while the zeroth-order Hamiltonian matrix is now defined as

$$\hat{H}_0 = \hat{P}_0 \hat{F} \hat{P}_0 + \hat{P} \hat{F} \hat{P} \tag{1.4.7}$$

$$\hat{P}_0 = |0\rangle\langle 0| \tag{1.4.8}$$

$$\hat{P} = \sum_{\mu} |\mu\rangle\langle\mu| \tag{1.4.9}$$

In the above equations, $|0\rangle$ indicates a reference state, D_{pp} the diagonal element of the one-particle density matrix for the p orbital, and ϵ an average shift parameter. The value of ϵ varies depending on the system between 0.25 and 0.30 a.u. Larger shifts cause shifting more up the potential energy curve in the dissociative region.

No shift is needed in the equilibrium geometry region of the potential energy curve.

1.5 Characterization of the Electronically Excited States and their Interaction

Excitation processes in a system composed of two chromophores, occurring for example in nucleic acids after the absorption of UV light, are the scope of this work. The following text gives the theoretical background for the interaction between the chromophores in their excited states, starting with a definition of an electronically excited state.

1.5.1 Character of Excited States

The orbitals of a system can be divided into core, valence and virtual orbitals. The core orbitals are fully occupied by electrons in the ground state of a system and have lower energies than the valence orbitals. The valence orbitals can be occupied fully or partially depending on the number of electrons. The virtual orbitals are unoccupied in a ground state.

Figure 1.1 qualitatively depicts the creation of molecular orbitals in formaldehyde molecule. On the left side of the figure, there are the core (below) and valence ($2sp^2$ and $2p_z$) orbitals of CH_2 and on the right side, there are the valence orbitals of oxygen atom (O). In the middle of the picture, there are the molecular orbitals σ(C-O), n(sp), π(C-O), $n(p_y)$, π^*(C-O), and σ^*(C-O) that are created from the valence orbitals. Figure 1.2, which is a qualitative energy diagram of the molecular orbitals of formaldehyde, helps to explain the meaning of the molecular orbital notification.

The molecular orbitals can be characterized according to their nodes as σ, π and lone pair (n, illustrated in Figure 1.3a) orbitals. The π (Figure 1.3b) and π^* (Figure 1.3c) orbitals are characterized by the node in the plane of the molecule, while there is no such node in σ and n orbitals. The molecular orbitals are then filled by electrons according to their energy which in the case of formaldehyde results in a closed-shell singlet state. In this case, n is the so-called Highest Occupied Molecular Orbital (HOMO). π denotes a bonding orbital with no nodes between the atoms forming the bond, as depicted in Figure 1.3b and π^* denotes an anti-bonding orbital

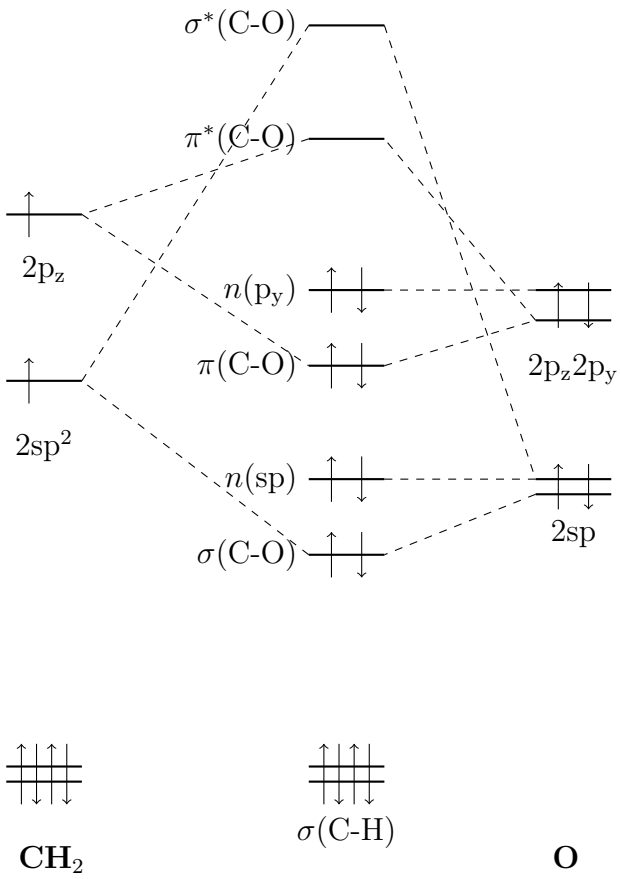

Figure 1.1: The qualitative diagram of the molecular orbitals creation in formaldehyde molecule.

having a node between the two atoms of the bond (see Figure 1.3c). π^* orbital is the Lowest Unoccupied Molecular Orbital (LUMO) in the formaldehyde molecule. In Figure 1.2, π and π^* are the occupied and the virtual orbitals, respectively.

The energetically low-lying excited states are formed by the promotion of an electron from either n or π bonding orbitals into π^* antibonding orbital, forming the $n \rightarrow \pi^*$ or $\pi \rightarrow \pi^*$ states, respectively. At higher energies the formation of states resulting from promotion from occupied σ and/or into virtual σ^* orbitals can be detected. The orbitals which are singly occupied are usually denoted SOMO (Singly Occupied Molecular Orbitals). The excited states can be further characterized according to the their spin quantum numbers. The parallel and antiparallel spin of the electrons in SOMO's result in the formation of triplet and singlet states, respectively.

The above described excitation processes are induced by the absorption of the energy in the range of 2-120 eV approximately, i.e. in the so-called UV-VIS region.

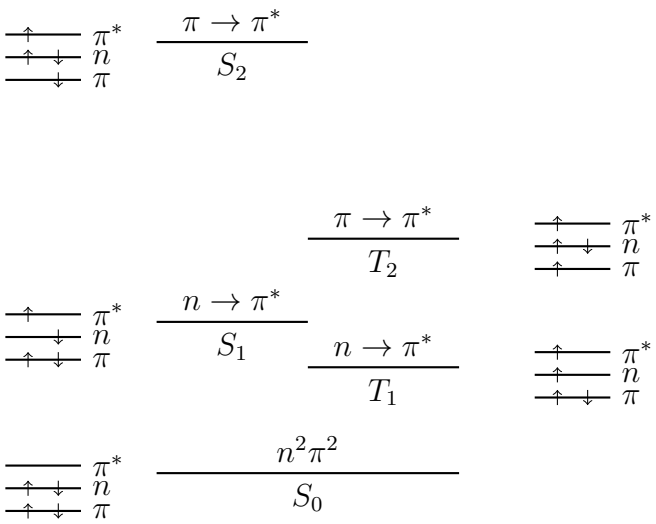

Figure 1.2: The qualitative energy diagram of formamide.

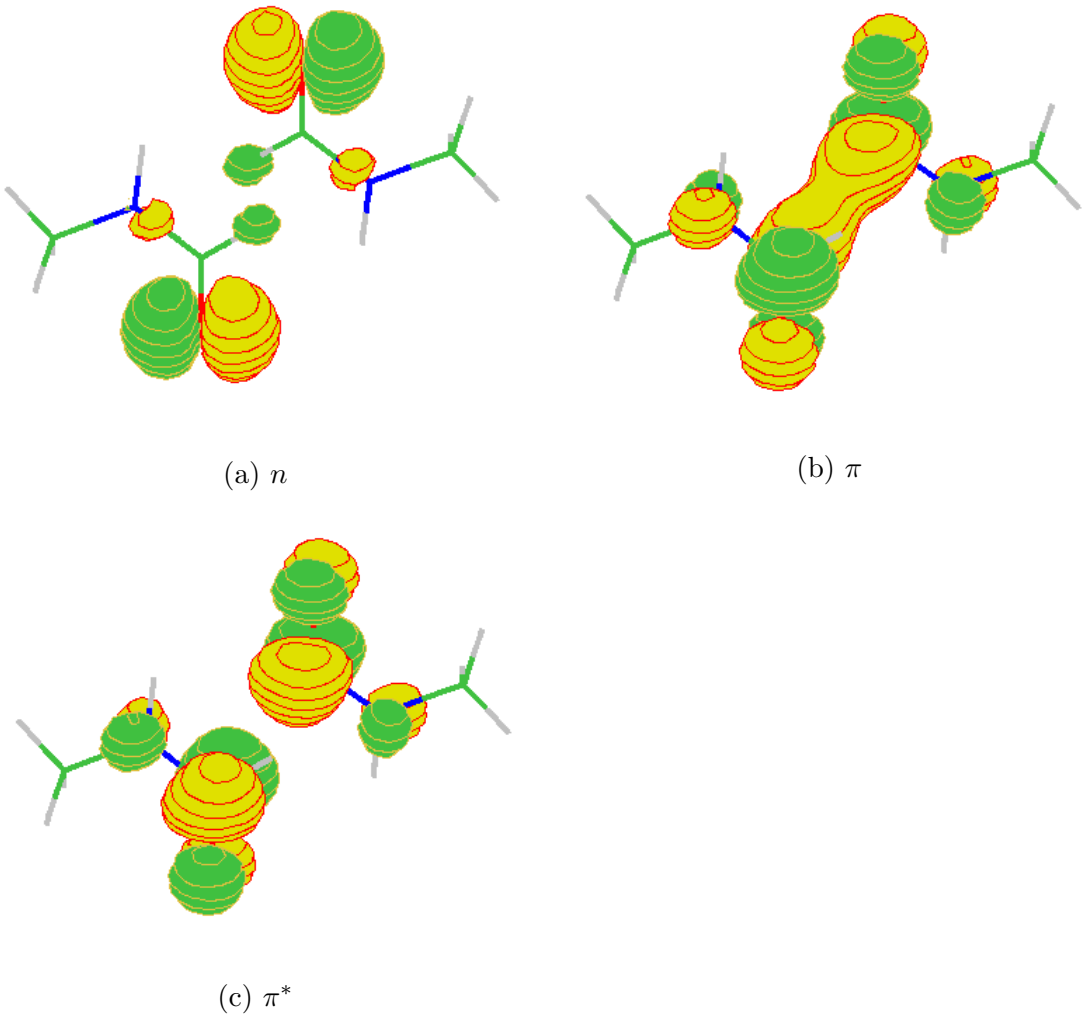

(a) n

(b) π

(c) π^*

Figure 1.3: (a) The non-bonding n, (b) the bonding π and the antibonding π^* orbitals. The blue are nitrogen atoms, the red the oxygen atoms, the green the carbon atoms, and the gray belongs to hydrogen. The different sign of the orbital function is distinguished by the yellow and green colors.

In addition to the electronic characterization, the excited states can be also characterized according to their intensity. The intensity I follows the so-called Beer-Lambert law

$$I = I_0 10^{-\varepsilon[M]l} \tag{1.5.1}$$

where I_0 denotes the intensity of the radiation colliding with the system, ε molecular absorption coefficient, $[M]$ the molar concentration of the system, and l the length of the system. ε depends on the frequency of the colliding radiation. The Beer-Lambert law has also the form

$$A = \log \frac{I_0}{I} = \varepsilon(\nu)[M]l \tag{1.5.2}$$

where A designates the absorbance of the sample M and the frequency ν of the colliding radiation. Since a colliding radiation usually contains more than one frequency, the corresponding physical meaning gives the oscillator strength

$$f \sim \int_{\nu_1}^{\nu_2} \varepsilon(\nu) d\nu = C|\mu_{fi}|^2 \tag{1.5.3}$$

where the absorbed radiation is from the interval $\langle \nu_1; \nu_2 \rangle$.

The allowance/forbiddance of transitions is given by the value of

$$\mu_{fi} = \langle \psi_f | \hat{\mu} | \psi_i \rangle \tag{1.5.4}$$

which is the transition moment between the initial state (described by the wavefunction ψ_i) and the final state (described by the wavefunction ψ_f). The relation between f and μ_{fi} is shown in Equation (1.5.3), where C denotes a constant. In Equation (1.5.4), $\hat{\mu}$ denotes the transition moment operator. The transition $\psi_i \to \psi_f$ is forbidden when μ_{fi} is zero.

In the BO approximation (Section 1.1), $\psi = \psi_e \psi_n$, where ψ_e denotes the electronic wavefunction and ψ_n the wavefunction of nuclei. Further, $\psi_e = \psi_r \psi_{spin}$ where ψ_r is the spatial wavefunction and ψ_{spin} the spin wavefunction. To sum up, one can write

$$\psi = \psi_r \psi_{spin} \psi_n \tag{1.5.5}$$

Due to the division of the wavefunction to its spin, spatial (or electronic) and nuclei (or vibrational) contributions, μ_{fi} can also be divided into these three parts. An allowed transition must have all these three contributions of μ_{fi} nonzero. Whether μ_{fi} is zero can be predicted by so-called selection rules without solving the transition moment. The selection rules differ depending on the nature of the transition.

When mostly the electric dipole interaction contributes to the transition, μ_{fi} in the BO and FC approximation can be rewritten to the form

$$\mu_{fi} = \left\langle \psi_n^f | \psi_n^i \right\rangle \left\langle \psi_e^f | \hat{\mu}_e | \psi_e^i \right\rangle \tag{1.5.6}$$

where $\left\langle \psi_n^f | \psi_n^i \right\rangle$ denotes the Franck-Condon overlap integral which describes how much ψ_n^f resembles ψ_n^i. When the resemblance is sufficiently large, the transition is favored by the nuclear motion. In $\left\langle \psi_e^f | \hat{\mu}_e | \psi_e^i \right\rangle$, where $\hat{\mu}_e$ indicates the electron dipole nature, one can use $\psi_e = \psi_r \psi_{spin}$ so that the dipole moment has the form

$$\mu_{fi} = \left\langle \psi_n^f | \psi_n^i \right\rangle \left\langle \psi_{spin}^f | \psi_{spin}^i \right\rangle \left\langle \psi_r^f | \hat{\mu} | \psi_r^i \right\rangle \tag{1.5.7}$$

The term $\left\langle \psi_{spin}^f | \psi_{spin}^i \right\rangle$ allows only transitions where the final state has the same multiplicity as the initial. In the language of selection rules, it means that $\Delta S = 0$ for the allowed transitions.

This is true in the zeroth-order approximation. However, in higher orders, the states are not with pure multiplicities, which allows also the transitions with different multiplicities. This happens when a so-called spin-orbit interaction is significant and one cannot write Equation (1.5.7).

In the zeroth-order approximation, the transition $S_0(n^2\pi^2) \rightarrow S_1(n, \pi^*)$ is forbidden due to the orthogonality of the n and π^* orbitals, which means no orbital overlap as can be seen from Figure 1.3. However, if vibrations that modify the shape of the orbitals instantaneously are considered, the orbital overlap increases. This sort of interaction, termed vibronic, can cause an allowance of the transition $S_0(n^2\pi^2) \rightarrow S_1(n, \pi^*)$ in the first-order approximation. In addition, other interactions can contribute to this allowance. If we consider a spin-forbidden transition

$S_0(n^2\pi^2) \rightarrow T_1(n, \pi^*)$, despite the vibronic interaction, a so-called spin-orbit interaction is necessary. On the other hand, the transition $S_0(n^2\pi^2) \rightarrow S_2(\pi, \pi^*)$ is allowed also in the zeroth order, since the π and π^* orbitals have a perfect orbital overlap and do not cancel due to the symmetry as it can be seen from Figure 1.3. According to the selection rules (non-zero orbital overlap, symmetry), the transition moment $\pi \rightarrow \pi^*$ is much bigger than $n \rightarrow \pi^*$.

1.5.2 Photophysical and Photochemical Processes

Once the system is excited from the ground state PES (defined in Section 1.1) to that of electronically excited state, it can undergo various processes, depending on the initial absorption energy, and the relative position and the shapes of the energy surfaces of other excited states. These processes are summarized in the so-called Jablonski diagram (Figure 1.4). An excited state can decay radiatively through a fluorescence or a phosphorescence, or non-radiatively through internal conversions (IC) or intersystem crossings (ISC). The fluorescence can in principle occurs between any states with the same spin multiplicity ($S_i \rightarrow S_j$ where $i > j$). The relaxation from higher excited states is, however, much faster than any other process. Thus with only a very few exceptions, the fluorescence proceeds from S_1 state (Kasha's rule). If the radiative transition occurs from a triplet excited state (usually T_1) to the singlet ground state, it is termed a phosphorescence. IC and ISC stand for non-radiative transitions between the states of the same and different multiplicities, respectively. As indicated in Figure 1.4, the vibrational relaxation is another mechanism how to release the energy.

The non-radiative processes occur in the region, where the PESs of two states (Ψ_1 and Ψ_2) approach each other. This region is termed unavoided or weakly avoided conical intersections (surface touchings), illustrated in Figure 1.5b. However, when two PESs approach but no jumps between the surfaces occur, the conical intersection is avoided. For example, the avoided conical intersections occur in diatomic molecules between two states of the same spin and the same electronic symmetry. In polyatomic molecules, conical intersections can be unavoided or weakly avoided even under conditions indicated above.

For a polyatomic system with F degrees of freedom, one can distinguish two

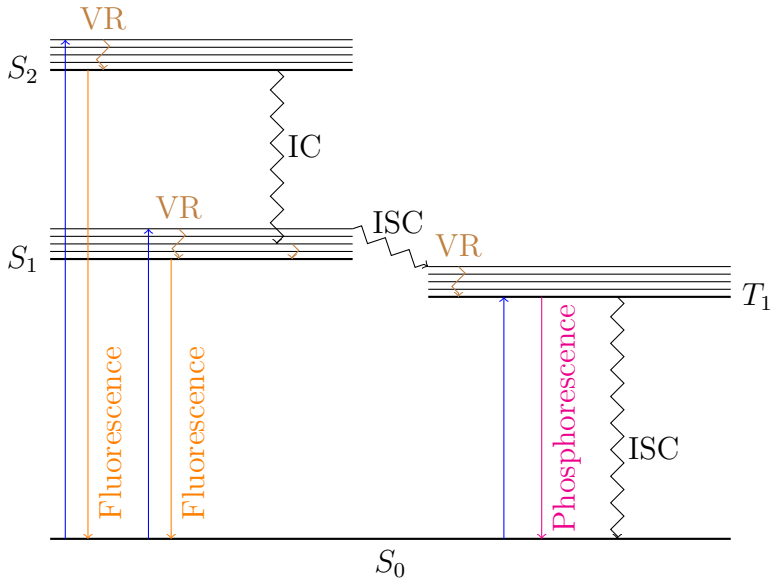

Figure 1.4: Jablonski diagram

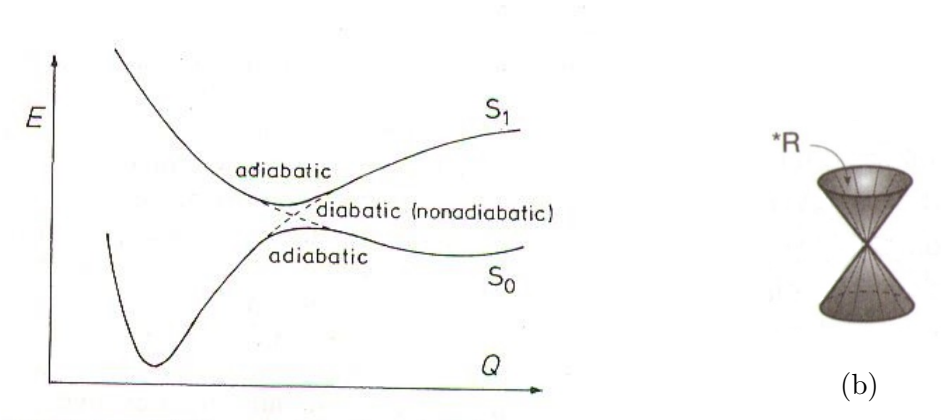

(a) (b)

Figure 1.5: (a) PES of a ground state and PES of a singlet excited state with adiabatic and diabatic (nonadiabatic) representations [35]. (b) A conical intersection.

subspaces: the intersection coordinate subspace with the $F-2$ dimensionality, and the branching space of 2 dimensionality ($\boldsymbol{x_1}$,$\boldsymbol{x_2}$). The first vector

$$\boldsymbol{x_1} = \frac{\partial(E_1 - E_2)}{\partial \boldsymbol{q}} \tag{1.5.8}$$

determines the direction in which the energy difference between the two states is the largest. The second vector

$$\boldsymbol{x_2} = \langle \Psi_1 | \frac{\partial \Psi_2}{\partial \boldsymbol{q}} \rangle \tag{1.5.9}$$

determines the direction in which the mixture of two adiabatic states is the largest.

An adiabatic state (ψ_1 or ψ_2) is a linear combination of diabatic states (ϕ_1, ϕ_2,...). For instance,

$$\psi_1 = c_{11}\phi_1 + c_{21}\phi_2 \tag{1.5.10}$$

$$\psi_2 = c_{12}\phi_1 + c_{22}\phi_2 \tag{1.5.11}$$

Adiabatic states are eigenstates of electrostatic Hamiltonian (1.0.4) and describes properly the processes in which nuclei move sufficiently slowly, i.e. the BO approximation is valuable. On the other hand, diabatic states are not eigenstates of electronic Hamiltonian (1.0.4) and are a reasonable approximation in the processes where nuclei move fast, which means the BO approximation fails. This is true in the region of conical intersections. Figure 1.5a illustrates the difference between the adiabatic and diabatic representations.

1.5.3 The Wavefunction of Interactive Chromophores

So far, excited states were described for monomer species only. However, my interest lies in interactions of two chromophores. The underlying theory for such case is outlined in the following text.

Let us consider a system of two chromophores A and B, each having two electrons. In its electronic ground state, the doubly occupied and virtual orbitals of chromophore $A(B)$ are denoted as $a(b)$ and $a^*(b^*)$, respectively. The wavefunction

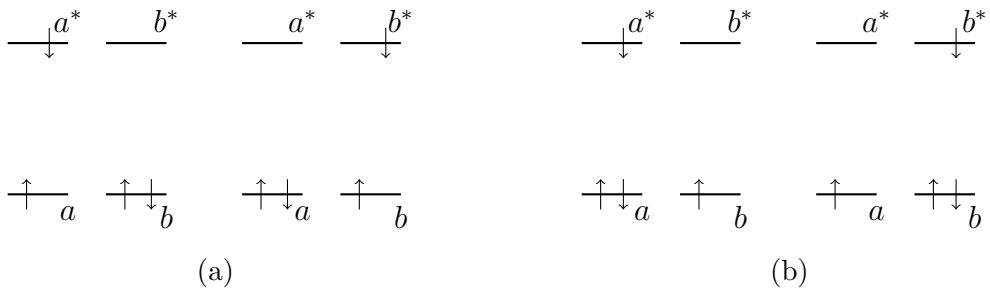

Figure 1.6: Configurations of (a) localized excitations $|A^*B\rangle$,$|AB^*\rangle$, and of (b) localized charges $|A^+B^-\rangle$, $|A^-B^+\rangle$.

of the ground state has the form

$$|\Psi_0\rangle = K\hat{A}|AB\rangle \tag{1.5.12}$$

where K is a normalization constant, $\hat{A}$ an operator that makes the wavefunction $|AB\rangle$ antisymmetric.

If we consider the system in its excited state with the excitation localized on one of the chromophores, there are two possible wavefunctions, depending on which chromophore the excitation is localized, $|A^*B\rangle$ and $|AB^*\rangle$:

$$|A^*B\rangle = N_1(|a\bar{a}^*b\bar{b}\rangle + |a^*\bar{a}b\bar{b}\rangle) \tag{1.5.13}$$

$$|AB^*\rangle = N_2(|a\bar{a}b\bar{b}^*\rangle + |a\bar{a}b^*\bar{b}\rangle) \tag{1.5.14}$$

where lines upon the spin orbitals mean spin down. The above functions represent localized excitations. N_i denotes a normalization constant. The functions are constructed from configurations indicated in Figure 1.6a

In the case of identical chromophores separated by a large distance, the excitations are localized and the energies of states are degenerated. In a closer position, the chromophores start to interact and the degeneracy is lifted. The split states have the following form of the wavefunctions

$$|\Phi_1^{\mathrm{ER}}\rangle = \frac{1}{\sqrt{2}}(|A^*B\rangle + |AB^*\rangle) \tag{1.5.15}$$

$$|\Phi_2^{\mathrm{ER}}\rangle = \frac{1}{\sqrt{2}}(|A^*B\rangle - |AB^*\rangle) \tag{1.5.16}$$

These states are also called the zeroth-order exciton resonance (ER) states. It has been showed that charge resonance (CR) states are important in the close-range interactions [56]. Their form is

$$|\Phi_1^{\mathrm{CR}}\rangle = \frac{1}{\sqrt{2}}(|A^-B^+\rangle + |A^+B^-\rangle) \tag{1.5.17}$$

$$|\Phi_2^{\mathrm{CR}}\rangle = \frac{1}{\sqrt{2}}(|A^-B^+\rangle - |A^+B^-\rangle) \tag{1.5.18}$$

where

$$|A^-B^+\rangle = K(|a\bar{a}b\bar{a}^*\rangle + |a\bar{a}a^*\bar{b}\rangle) \tag{1.5.19}$$

$$|A^+B^-\rangle = K(|a\bar{b}^*b\bar{b}\rangle + |b^*\bar{a}b\bar{b}\rangle) \tag{1.5.20}$$

are indicated in Figure 1.6b.

It is reasonable to expect that an excited-state wavefunction depends mostly on the exciton resonance and the charge resonance states. Thus, we can write

$$|\Psi^*\rangle = c_1|\Phi_1^{\mathrm{ER}}\rangle + c_2|\Phi_2^{\mathrm{ER}}\rangle + c_3|\Phi_1^{\mathrm{CR}}\rangle + c_4|\Phi_2^{\mathrm{CR}}\rangle \tag{1.5.21}$$

1.5.4 Electronic Coupling

In previous Section 1.5.3, an approximate wavefunction of an electronically excited state of two chromophores was stated. If we now consider $\Phi_1^{\mathrm{ER}}, \Phi_2^{\mathrm{ER}}, \Phi_1^{\mathrm{CR}}, \Phi_2^{\mathrm{CR}}$ to be a basis set, we can obtain the Hamiltonian matrix in this basis set

$$H = \begin{pmatrix} H_{11} & H_{12} & H_{13} & H_{14} \\ H_{21} & H_{22} & H_{23} & H_{24} \\ H_{31} & H_{32} & H_{33} & H_{34} \\ H_{41} & H_{42} & H_{43} & H_{44} \end{pmatrix} \tag{1.5.22}$$

Every non-diagonal element of the Hamiltonian matrix H is termed an electronic

coupling, denoted as u, and represents interactions between the chromophores. The higher the electronic coupling is, the stronger the interactions are.

The electronic coupling can be expressed as a sum of a short-range u_{short} and long-range contributions. The long-range contributions represent Coulombic interactions u_{Coul}.

$$u = u_{\text{short}} + u_{\text{Coul}} = u_{\text{pen}} + u_{\text{exch}} + u_{\text{Coul}} \tag{1.5.23}$$

The short-range term contains a penetration interaction u_{pen} and the quantum mechanical exchange interaction u_{exch}. The penetration interaction represents the interaction of an electron on one molecule with the charge density of the other molecule, and the exchange interaction represents a quantum-mechanical feature with no classical analogy. The short-range term has been ascertained to have exponential dependence on the interchromophore separation R due to the strong dependence on the orbital overlap. The exponential dependence entails that the short-range term becomes negligible at separations larger than 6 Å [56].

The Coulombic term can be expanded to a multipole expansion of dipole-dipole, dipole-octopole and octopole-octopole, etc. interactions [56]

$$u_{\text{short}} = u_{\text{d-d}} + u_{\text{d-o}} + u_{\text{o-o}} + \cdots \tag{1.5.24}$$

In the expansion, the dipole-dipole term usually dominates. Thus, the electronic coupling in large separations can be approximated as a function with R^{-3} dependence. The other terms can decrease or increase the resultant u_{short} depending on the relative orientation of the chromophores.

1.5.5 Excitation Processes

The following processes can happen after excitation of two chromophores [35]:

- localization of the excitation on one chromophore
- delocalization of the excitation forming an exciton
- strongly interacting complexes termed exciplexes/excimers
- electron or proton transfer (sometimes called charge transfer (CT))

- excitation energy transfer (EET)
- formation of one or more new photoproducts

Two of them have been already mentioned: the localization of the excitation on one chromophore and electron or proton transfer. These can be described by the localization excitations Φ_1^{ER}, Φ_2^{ER} and by the charge resonance states Φ_1^{CR}, Φ_2^{CR}. In addition to these two cases, new terms were introduced. An exciplex/excimer wavefunction has been already suggested in Subsection 1.5.3 in wavefunction (1.5.21) if all four terms contribute to the interactions. An excimer is an excited dimer (or multimer) of identical chromophores, while an exciplex of two (or more) nonidentical molecules. From this point, I will refer to the excimer term since the focus of this work is on identical chromophores. The stability of an excimer is controlled mostly by the orbital overlap, i.e. u_{short} dominates in formation of an excimer. The final wavefunction is characterized by contributions from the electronic configurations with electron promotion between the orbitals delocalized between the two chromophores, or CR configurations. The exciton, on the other hand, can be described in terms of ER configurations, forming so-called Frenkel exciton introduced in the Frenkel theory [25, 20]. In the case when also orbital overlap contributes, the wavefunction of the exciton can be expressed as a linear combination of ER and CR configurations.

Thus, overlap effects contribute also to interactions of molecular excitons and to EET (Equation (1.5.25)) occurring when the chromophores' distance is between $3-6$ Å [56].

$$A^* + B \rightarrow A + B^* \tag{1.5.25}$$

However, EET are formed mostly by the interactions of the intermediate regime.

Each of the five explained processes can initiate a photochemical reaction leading to new photoproducts. It is hard to predict whether the localization of excitation on one chromophore or delocalization prevents a photochemical reaction. This is specific to every system, its character of the excited state, and its geometry.

1.6 The Surface Hopping Dynamics

Excitation processes include photochemical reactions, and radiative and non-radiative decays. The non-radiative decays entail a change of the electronic state in the geometry. These non-radiative decays belong to non-adiabatic processes for which a non-adiabatic dynamics is necessary.

A non-adiabatic dynamics allows population changes in an electronic state where a wavefunction is a linear combination of adiabatic or diabatic states

$$\Psi(\mathbf{r}, \mathbf{R}, t) = \sum_i c_i(t)\varphi_i(\mathbf{r}, \mathbf{R}) \tag{1.6.1}$$

where $\varphi_i(\mathbf{r}, \mathbf{R})$ depends on the coordinates of electrons $\mathbf{r}$ and parametrically on the coordinates of nuclei $\mathbf{R}$. Since the adiabatic states ψ_i are not eigenstates of the nuclei kinetic operator, the terms $\langle\psi_i|\nabla_m\psi_j\rangle$ and $\langle\psi_i|\nabla_m^2\psi_j\rangle$ are nonzero in the adiabatic representation. If a diabatic representation ϕ_i is used, the terms $\langle\phi_i|\nabla_m\phi_j\rangle$ and $\langle\phi_i|\nabla_m^2\phi_j\rangle$ are minimized, and the terms $H_{ij} = \langle\phi_i|\hat{H}_e|\phi_j\rangle$ become nonzero. $\hat{H}_e$ denotes the electronic part of the Hamiltonian (1.0.4), which entails $\hat{H}_e = \hat{T}_e + \hat{V}_{ee} + \hat{V}_{en}$.

The non-adiabatic processes cannot be fully described by any static computation. Static computations allow to find excited state minima and conical intersections, but they do not allow to fully explore the configurational space, and to determine the lifetime of an excited state. This can be done through a non-adiabatic dynamics which solves the time-dependent Schrödinger equation (1.0.1). After including expansion (1.6.1) into the Schrödinger equation (1.0.1), one obtains

$$i\hbar\frac{\partial c_k}{\partial t} = \sum_i c_i \left(\langle\varphi_k(\mathbf{r}, \mathbf{R})|H_e|\varphi_i(\mathbf{r}, \mathbf{R})\rangle - i\hbar\langle\varphi_k(\mathbf{r}, \mathbf{R})|\nabla_m\varphi_i(\mathbf{r}, \mathbf{R})\rangle\frac{\partial R}{\partial t}\right) \tag{1.6.2}$$

where the term of the second order is neglected. This equation can be rewritten to the form

$$i\hbar\frac{dc_k}{dt} + \sum_j(-H_{kj} + i\hbar\mathbf{F}_{kj}^m \cdot \mathbf{v}^m)c_j = 0 \tag{1.6.3}$$

where

$$H_{kj}(\mathbf{R}) = \langle \varphi_k | H_e | \varphi_j \rangle \tag{1.6.4}$$

and $\mathbf{F}_{kj}^m$ is the nonadiabatic coupling vector defined as

$$\mathbf{F}_{kj}^m = \langle \varphi_k | \nabla_m | \varphi_j \rangle \tag{1.6.5}$$

then, $\mathbf{v}^m$ is the velocity operator for atom m with the mass M_m

$$\mathbf{v}^m = -i\hbar \frac{\nabla_m}{M_m} \tag{1.6.6}$$

Equation (1.6.3) is solved at the each step of the dynamics and can be called a local time-dependent Schrödinger equation. The resultant c_k coefficients, however, need a correction, because Equation (1.6.3) forces the system evolve in one direction but "every time" it is a different trajectory. In other words, if we start the dynamics several times from the same initial geometry, every time we obtain a different trajectory. This is called a decoherence effect and in order to correct it, these three equations

$$c_k' = \exp\left(-\frac{\Delta t}{\tau_{kl}}\right) \tag{1.6.7}$$

$$c_l' = c_l \sqrt{\frac{1 - \sum_{k \neq l} |c_k'|}{|c_l|^2}} \tag{1.6.8}$$

$$\tau_{kl} = \frac{\hbar}{|V_{kk} - V_{ll}|} \left(1 + \frac{\alpha}{E_{\text{kin}}}\right) \tag{1.6.9}$$

are solved every time. In the equations, l denotes the current state, E_{kin} the kinetic energy of nuclei, Δt the time through the integration has been performed, and α an empirical parameter, usually equal 0.1 hartree. In Equation (1.6.7), $k \neq l$.

Since a non-adiabatic dynamics is computationally demanding, several approximate methods were developed. One of them, called Surface Hopping Dynamics, has been employed in this work.

The surface hopping approach means the usage of adiabatic representation and solving these two Newton's equations (together with Equation (1.6.3)):

$$\frac{d^2\mathbf{R}_m}{dt^2} - \frac{\mathcal{F}_m}{M_m} = 0 \tag{1.6.10}$$

$$\mathcal{F}_m = -\nabla_m V_l \tag{1.6.11}$$

where $\mathbf{R}_m$ is the trajectory of atom m, M_m the reduced mass, $\mathcal{F}_m$ the force on atom m, and V_l is the potential energy of a single state l.

Before the dynamics starts, different initial guesses are made. This enables to explore the configurational space in various directions. Further, allowing to jump to a lower energy surface helps to gain a reasonable distribution.

The Surface Hopping Dynamics evaluates the transition probabilities between each two electronic states l and k

$$P_{l\to k} = \frac{\text{population decrease in } k \text{ due to the population increase in } l \text{ during } \Delta t}{\text{population of } l} \tag{1.6.12}$$

in the adiabatic representation [7]. They can be evaluated by several methods. The most common approach is the Fewest-Switches method proposed by Tully [67] in which the transition probabilities in the adiabatic representation can be approximated as

$$P_{l\to k} = \max[0, \frac{-2\Delta t}{\rho_{ll}} \mathrm{Re}(\rho_{kl}) \mathbf{F}^m_{kl} \cdot \mathbf{v}^m] \tag{1.6.13}$$

where $\rho_{kl} = c_k c_l^*$.

When the transition probabilities are known, the computer program decides if the system hops to another surface. The decision is made when two conditions are fulfilled. Firstly, the program generates a random number r_t in time t. This number is from the interval $\langle 0, 1\rangle$. If the number satisfies the condition

$$\sum_{n=1}^{k-1} P_{l\to n}(t) < r_t \leq \sum_{n=1}^{k} P_{l\to n}(t) \tag{1.6.14}$$

and if also the second condition has the form

$$V_k(\mathbf{R}(t)) - V_l(\mathbf{R}(t)) \leq \frac{(\sum_m^{N_{at}} \mathbf{v}_m \cdot \mathbf{F}_{kl}^m)^2}{2\sum_m^{N_{at}} M_m^{-1}(\mathbf{F}_{kc}^m)^2} \tag{1.6.15}$$

is fulfilled, the system hops to the other surface.

The second condition forbids any increase in the total energy after the jump. This condition can differ when $\mathbf{F}_{kl}^m$ is not calculated directly during the dynamics procedure. Then the second condition

$$V_k(\mathbf{R}(t)) - V_l(\mathbf{R}(t)) \leq E_{kin}(\mathbf{v}) \tag{1.6.16}$$

where E_{kin} is the nuclear kinetic energy.

In this work, the non-adiabatic dynamics with the surface hopping algorithm has been performed in the *Newton-X* program. This program follows these points in the dynamics:

1. solving the time-independent electronic Schrödinger equation in order to obtain energies. Then, the program calculates their gradients, and nonadiabatic couplings. The non-adiabatic couplings are evaluated only when the energy difference between the surfaces is lower than a pre-defined value.

2. integrating the local time-dependent Schrödinger equation (1.6.3) for the nuclei in order to obtain c_i coefficients. This coffecients are then modified by decoherence corrections (1.6.7)-(1.6.9). Having the coefficients, one can evaluate the transition probabilities and perform the stochastic algorithm determining the current state.

3. solving the Newton's equations (1.6.10)-(1.6.11), which means that the nuclear motion is handled by the classical molecular dynamics.

4. repeating the procedure 1-3 until the end of the trajectory.

Chapter 2

N-Methylformamide

In this work, excitation processes in the N-methylformamide dimer have been examined. The following section explains my motivation to study this system. Then, I report my results.

2.1 Why N-Methylformamide

The understanding of excitation processes is one of the main task of physicists and chemists not only for fundamental academic reasons but also they are important factors in biological systems or industrial materials. The focus of this work is on excitation processes occurring between the chromophores. Such processes can occur whenever there is a suitable mutual orientation between the chromophores. A typical case of such systems are nucleic acids: deoxyribonucleic acid (DNA), ribonucleic acid (RNA).

The DNA is characterized by primary, secondary, tertiary, and quaternary structure. The primary structure gives the sequence of nucleotides (nucleobase and deoxyribose) linked through phosphates (illustrated in Figure 2.1). There are five nucleobases which naturally appear in nucleic acid structures: based on pyrimidine (cytosine (C), thymine (T) and uracil (U)) and purine type (adenine (A) and guanine (G)). DNA is composed of C, T, A and G, while RNA obtains C, U, A and G.

The secondary structure is given by an organization of the polynucleotide in the space. DNA has typically a double-stranded right-handed helical structure, while

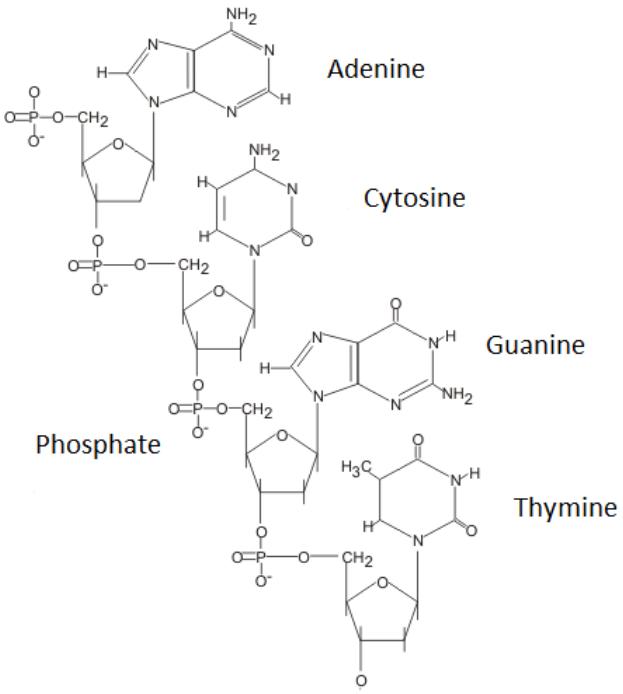

Figure 2.1: A single strand of DNA.

RNA is single-stranded. The interactions between the two strands are mediated by hydrogen bonds between a pyrimidine base on one strand and a purine base on a complementary strand. This gives the A-T and G-C pairing, a base of the transfer of genetic information. Depending on the conditions (ionic strength, solvent, etc), DNA can form into different conformations, e.g. right-handed B-DNA or A-DNA (the arrangement of bases similar as in RNA) or left-handed Z-DNA. Nucleic acids can form a more complex helical arrangement, the so-called tertiary structure, such super-helical arrangements, or structures in complexes with other bio-molecules, such as nucleosomes or chromosomes, called quaternary structures.

Within the helical structures, the arrangements of adjacent bases allow for strong stacking interactions. As this type of interactions was found to be dominant in the excited-state processes in DNA, I have chosen them as the target of my study.

Excitation processes of nucleobases have been examined, for example, in [1]-[4],[10, 13],[15]-[18],[34, 39, 43, 45, 47, 50, 52, 64, 68, 69]. It has been showed that the lifetime of the excited states of the all isolated nucleobases occurring in DNA or RNA are very short (on the picosecond or sub-picosecond time scale)[13, 68] in comparison to much longer lifetimes of other compounds with a similar chemical

constitution [9, 13]. The short lifetime of nucleobases acts as a protection mechanism against nucleic acids UV-damage. The photophysics of nucleobases become, however, much more complicated when they are embedded in DNA molecule. The experimental observations were interpreted by existence of both, short-lived events, similar to those observed for isolated species, and long-lived processes appearing on up to nano-second timescales [11, 17, 18, 39, 43, 51, 69]. This elongation increases the probability of chemical changes (photochemical processes) which can modify the genetic code. For example, two adjacent pyrimidines in stacking conformation can dimerize to form cyclobutane pyrimidine dimers after UV radiation. The corresponding cycloaddition is the example of the reaction forbidden in the ground state but allowed in the excited state, similarly as two ethylene molecules to cyclobutane [12]. Importantly, the presence of cyclobutane thymine dimers is connected with the appearance of the skin cancer [28].

The character of the system, i.e. its complexity and size, requires step-by-step studies performed on smaller model systems. One of the problems, which have not been elucidated so far, is the character of the excited state interactions between two stacked chromophores. The model system ought to have the same character of its excited states as the nucleobases have: $n \rightarrow \pi^*$ and $\pi \rightarrow \pi^*$. The smallest systems which have these characters of their excited states are formaldehyde and formamide. Since the former easily dissociate after the excitation, the later system was used for studies in the present work. In addition, the optimization of formamide dimer resulted in the hydrogen bonded structures. Thus, to maintain the stacking interactions, the formamide was methylated at N atom. The beginning of the following section describes the chosen model system in detail.

To obtain a full description of the excited state behavior, both "static" and dynamical calculations need to be performed. The former constitute of the calculations of the critical points on the PES, i.e. vertical excitation energies in the FC region, the energies and geometries of excited state minima and structures on the crossing seams. These calculations are then followed by dynamics simulations performed at the level which has been chosen based on the results of static calculations.

2.2 Computational Details

2.2.1 Ground State

As mentioned in the previous section, the optimization of formamide dimer led to the formation of hydrogen bonded complex. For this reason, I modified the system by the methylation in which the hydrogen atoms of amino groups were replaced by methyl groups. The following systems were considered:

- N,N-dimethylformamide dimer (NN-dMF dimer)
- N,N-dimethylformamide dimer with one water molecule (NN-dMF-w dimer)
- C,N-dimethylformamide dimer with two water molecules (CN-dMF-2w dimer)
- N-methylformamide dimer with two water molecules (MF-w dimer)

The ground state of all species were optimized at the MP2/6-311G* [37, 44] level by *Gaussian09* [26]. The ground state calculations of N-methylformamide (MF) monomer and the monomer with one water molecule (MF-w) were supplemented at the same level.

2.2.2 Vertical Excitations

The vertical excitations of MF and MF-w monomers were calculated by the SA-3-CASSCF method employing (4,5) and (6,5) active spaces and the 6-31G* basis set [29, 30].

The vertical excitations of MF-w dimer were calculated using the SA-3-CASSCF and SA-5-CASSCF methods. To correct for the dynamic correlation effects, the MS-CASPT2 single point calculations were performed with or without various imaginary shifts. I employed the 6-31G* and 6-311G* basis sets varying the active space from (8,8) to (12,10). The SA-3-CASSCF(8,10)/6-31G* level has been chosen for further computations giving the correct characters of the singlet excited states (see results in Subsection 2.3.2).

To evaluate the effect of water molecules on the excited state energies, the MF dimer system was also calculated.

The *Molcas* program [32, 46, 70] has been used to calculate the vertical excitation energies.

2.2.3 Adiabatic Excitations and Conical Intersections

The excited state minima and conical intersections of the MF-w monomer and of the MF-w dimer were searched by the SA-3-CASSCF employing the 6-31G* and 6-311G*, respectively. Then, the MS-CASPT2 single point calculations were performed in order to obtain the dynamic correlation. The imaginary shift 0.3 was employed.

For the geometry optimization of the excited states and the conical intersection searches, the *Columbus* program [14, 40, 41, 58] was used. The following MS-CASPT2 calculations were performed by the *Molcas* program [32, 46, 70].

2.2.4 Non-Adiabatic Dynamics

The non-adiabatic dynamics with the surface hopping algorithm was performed at the CASSCF(8,10) level employing the 6-31G* basis set. The dynamics simulations ran for hundred trajectories starting from S_2. The time step was set 0.5 fs but then adjusted to the 0.2 fs in the trajectories that required a decreased time step due to a close conical intersection.

For the dynamics, the *Newton-X* program [5, 6] has been used, with the use of the *Columbus* program for the calculations of energies, energy gradients, and non-adiabatic coupling vectors. The initial geometries were generated by the Wigner distribution using the frequencies calculated at the B3LYP/6-31G* level in the *Turbomole* program [37, 44, 65, 71].

2.3 Results

2.3.1 Ground State

Two conformers, trans and cis, of MF were detected experimentally, with the former being more stable in the gas phase [60] and in the solution [66]. The optimized form

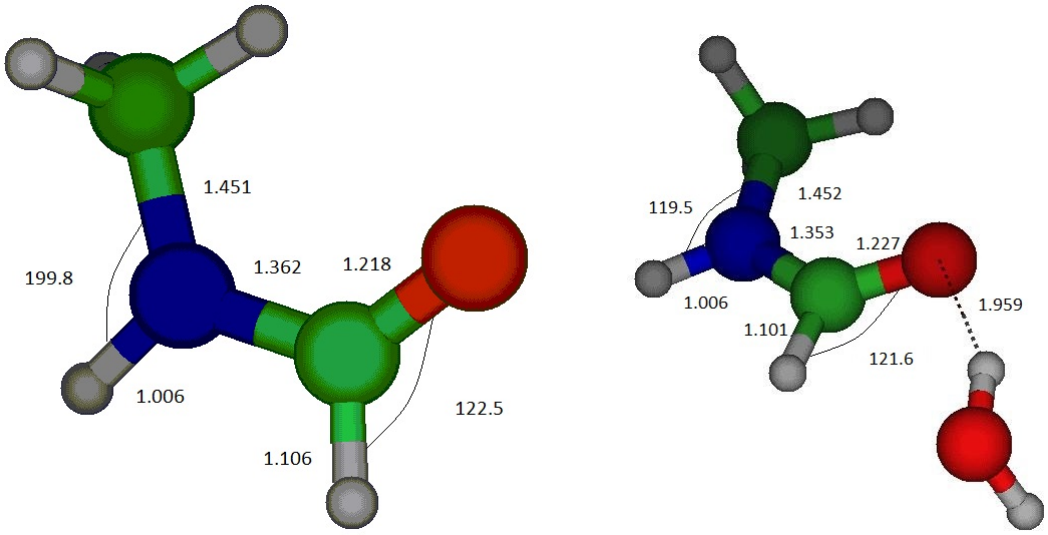

(a) MF

(b) MF-w

Figure 2.2: The ground state geometries of (a) MF at the MP2/6-311* level with the energy -208.007540 a.u. and of (b) MF-w at the same level with the energy -284.050462 a.u. The distances are in Å and the angles in degrees.

of this conformer (MF) and in the cluster with water (MF-w) is shown in Figure 2.2.

The ground state geometries of the systems originally considered for the dynamics computation are illustrated in Figures 2.3-2.6. All the dimer models resulted in a stacking geometry; however, NN-dMF-w dimer ended in a partially open structure (illustrated in Figure 2.4) to the space which could result in disrupting of the stacking conformation during a dynamics simulation. Thus, the structure was not considered in the further computations. The presence of two water molecules in CN-dMF-2w and MF-w dimers seemed to be a reliable step in obtaining a stable stacking geometry during a dynamics simulation. CN-dMF-2w dimer, however, showed up to dissociate in a CI search. Therefore, only MF-w dimer was further considered.

2.3.2 Potential Energy Surface of MF-w Dimer

The vertical excitation energies of MF and MF-w monomers are summarized in Table 2.1. In agreement with the previous calculations, the first and second excited states of MF are of $n \rightarrow \pi^*$ and $\pi \rightarrow \pi^*$ characters, respectively. The energies of the first excited states of MF and MF-w monomers do not differ by more than 0.2

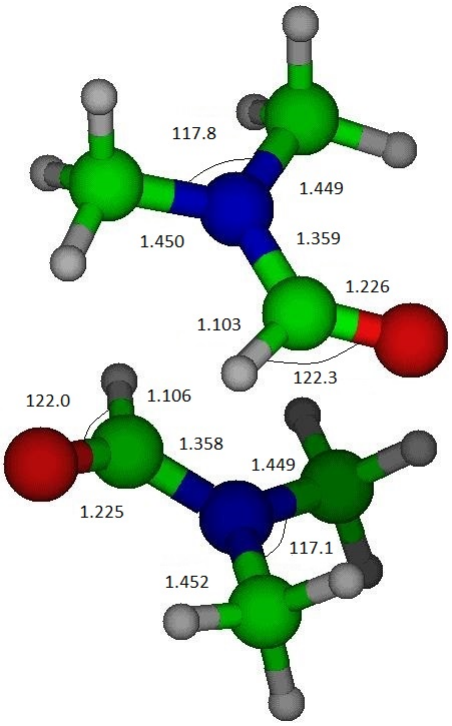

Figure 2.3: The ground state geometry of NN-dMF dimer at the MP2/6-311G* level with the energy -495.648747 a.u. The distances are in Å and the angles in degrees.

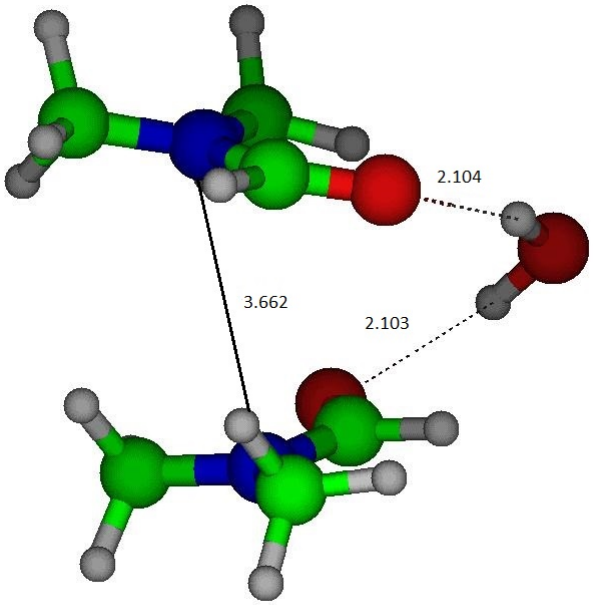

Figure 2.4: The ground state geometry of NN-dMF-w dimer at the MP2/6-311G* level with the energy -571.900119 a.u. The distances are in Å and the angles in degrees.

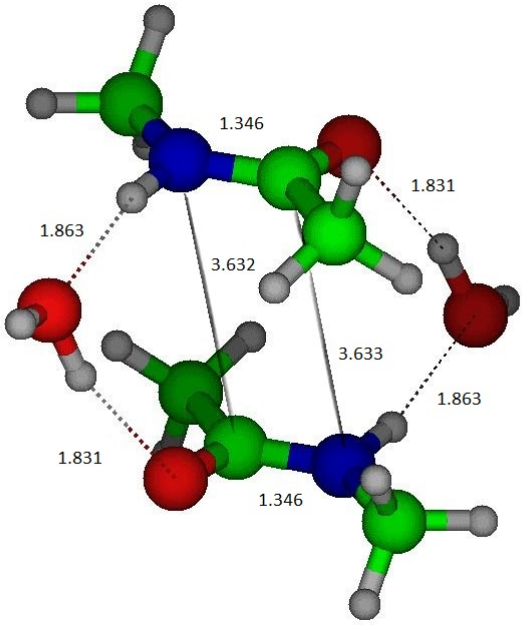

Figure 2.5: The ground state geometry of CN-dMF-2w dimer at the MP2/6-311G* level with the energy -648.200782 a.u. The distances are in Å and the angles in degrees.

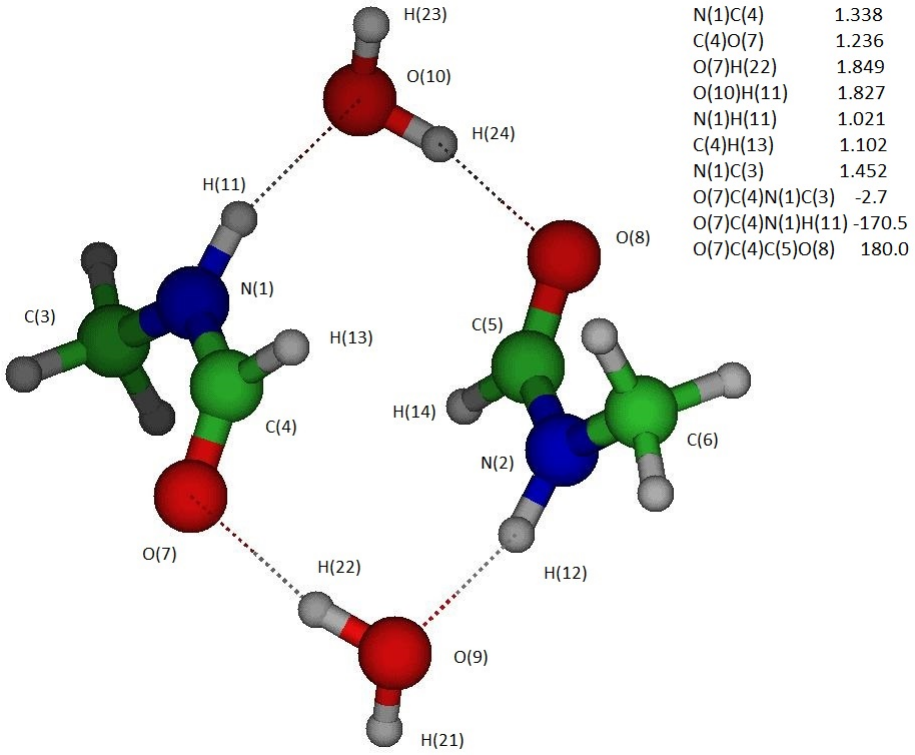

Figure 2.6: The ground state of MF-w dimer at the MP2/6-311G* level with the energy -569.817502 a.u. The distances are in Å and the angles in degrees. The parameters of the second monomer are the same.

eV, regardless of the size of the active space and the method used. High energies of the second excited state reflect a well-known deficiency of the CASSCF method to account for correlation effects. Inclusion of these effects in the MS-CASPT2 method improves these energies when sufficiently large active space is used. The MS-CASPT2 excitation energies are, however, still too large when the smaller (4,5) active space is used. Since the goal of our studies is the observation of the states of $n \rightarrow \pi^*$ character, the SA-CASSCF(4,5) is sufficient. Note that the larger excitation energies obtained at the SA-5-CASSCF(12,10) level are due to the inclusion of the $\pi \rightarrow \pi^*$ state in the averaging procedure. Including one water molecule (MF-w monomer) causes a small blueshift (0.2-0.3 eV) in $n \rightarrow \pi^*$ energies, in agreement with previously reported studies [8, 36, 62]. Very small redshifts of $\pi \rightarrow \pi^*$ energies were obtained, too. In CAS(4,5), the redshift is 0.09 eV at the CASSCF level and 0.07 eV at the MS-CASPT2 level. In CAS(6,5), the redshift is 0.02 eV at both CASSCF and MS-CASPT2 levels. The redshift has been already observed for example in [8, 62].

The vertical excitations of MF and MF-w dimers were obtained at the SA-3-CASSCF and SA-5-CASSCF levels varying the active space from CAS(12,10) to CAS(8,10) and the basis set from the 6-31G* to the 6-311G*. From Table 2.1, it can be seen that S_2 and S_1 are degenerate in the vertical region with the delocalized $n \rightarrow \pi^*$ character. The MS-CASPT2 method decreased the energies by 0.2-0.4 eV. Importantly, the relative energies do not strongly depend on the following: the basis set, the method, the active space. In both models, S_3 and S_4 states are of $\pi \rightarrow \pi^*$ character delocalized between the two monomers. For these states, the degeneracy is removed. As expected, significant lowering of the excitation energies at the MS-CASPT2 compared to the CASSCF method was observed for these states.

The presence of water molecules in the dimer affects the excited state energies in the same manner as observed in the case of the monomer, i.e. the blueshift and redshift were observed in $n \rightarrow \pi^*$ and $\pi \rightarrow \pi^*$ states, respectively. The blueshift is around 0.3 eV regardless of CAS size or the basis set. The redshift is around 0.2 eV at both SA-5-CASSCF and MS-CASPT2 levels in CAS(12,10) and the 6-311G* basis set. Note that all the computed states in the vertical region have a bonding π orbital (illustrated in Figure 1.3b) between the carbons of the two monomers.

The energies of excited state minima of MF and MF-w monomers are given in Table 2.2. Both models preserved their characters from the vertical region: S_2 with $\pi \rightarrow \pi^*$ character and S_1 with $n \rightarrow \pi^*$ character. Importantly, the energy of $n \rightarrow \pi^*$ state agrees within 0.22 eV and after the inclusion of the correlation effect within only 0.06 eV. The blueshift in MF-w monomer in comparison to MF monomer is 0.17 and 0.25 eV at the MCSCF and MS-CASPT2 levels, respectively. The redshift is 0.14 and 0.18 eV at the MCSCF and MS-CASPT2 levels, respectively.

The geometrical parameters of S_1min of MF and MF-w monomers are illustrated in Figure 2.7. After comparing the geometry parameters summarized in Table 2.3, it can be seen that the excitation to $n \rightarrow \pi^*$ state is characterized by the distortion the C-N bond from 3.7° to 53.7° and the elongation of the CO bond from 1.228 Å to 1.369 Å.

The results of energy calculations of the excited state minima of MF-w dimer obtained at the SA-3-CASSCF level employing CAS(8,10) with the 6-31G* and 6-311G* basis sets are given in Table 2.2 and the corresponding geometrical parameters in Table 2.3. Note that the minimum of S_2 in the 6-31G* was not found despite the efforts. Both minima are of $n \rightarrow \pi^*$ character but in the excitation energy is localized on one monomer in S_1min and delocalized in S_2min regardless of the basis set. The results indicate that degeneracy from the vertical region was lifted.

The inspection of the molecular orbitals of S_1 state of MF-w dimer shows that in this state the excitation is localized on one of the monomer subunit. This subunit reflects the same geometry changes as found for MF and MF-w, i.e. a significant prolongation of one CO bond (from 1.236 Å to 1.424 Å) and large distortion around CN bond (from −2.7° to −59.8°). These parameters change only very little for the second monomer subunit. Contrary to that, the excitation is delocalized in S_2 state and both CO bond distances increase by 0.05 Å. The localization of S_1 state is reflected also by the excited monomer and stays almost unaffected in the case of the "ground-state" monomer. In S_2 state, both monomers are distorted by about the same amount (approx. 20°).

The conical intersection search of MF-w dimer was performed at the SA-3-CASSCF level with CAS(8,10) in the 6-31G* and 6-311G* basis sets. For these geometries, MS-CASPT2 single point calculations were performed. The energies

	E_1	E_2	E_3	E_4
MF	$n \rightarrow \pi^*$	$\pi \rightarrow \pi^*$		
SA-3-CASSCF(4,5)/6-31G*	6.01	9.97	-	-
MS-CASPT2	5.97	8.79	-	-
SA-3-CASSCF(6,5)/6-31G*	6.07	8.40	-	-
MS-CASPT2	5.98	7.62	-	-
Experiment [33]	-	7.08-7.22	-	-
Reference [19]	6.00	7.39	-	-
MF-w	$n \rightarrow \pi^*$	$\pi \rightarrow \pi^*$		
SA-3-CASSCF(4,5)/6-31G*	6.20	9.88	-	-
MS-CASPT2	6.15	8.72	-	-
SA-3-CASSCF(6,5)/6-31G*	6.27	8.38	-	-
MS-CASPT2	6.17	7.60	-	-
MF dimer	$n \rightarrow \pi^*$	$n \rightarrow \pi^*$	$\pi \rightarrow \pi^*$	$\pi \rightarrow \pi^*$
	D	D	D	D
SA-3-CASSCF(8,10)/6-31G*	5.89	5.89	-	-
MS-CASPT2	5.71	5.72	-	-
SA-3-CASSCF(12,10)/6-31G*	5.87	5.88	-	-
MS-CASPT2	5.59	5.60	-	-
SA-5-CASSCF(12,10)/6-311G*	6.12	6.12	8.60	8.79
MS-CASPT2	5.74	5.74	7.20	7.27
MF-w dimer	$n \rightarrow \pi^*$	$n \rightarrow \pi^*$	$\pi \rightarrow \pi^*$	$\pi \rightarrow \pi^*$
	D	D	D	D
SA-3-CASSCF(8,10)/6-31G*	6.23	6.23	-	-
MS-CASPT2	6.01	6.02	-	-
SA-3-CASSCF(8,10)/6-311G*	6.23	6.24	-	-
MS-CASPT2	5.93	5.93	-	-
SA-3-CASSCF(12,10)/6-31G*	6.20	6.21	-	-
MS-CASPT2	5.89	5.90	-	-
SA-3-CASSCF(12,10)/6-311G*	6.21	6.21	-	-
MS-CASPT2	5.83	5.83	-	-
SA-5-CASSCF(12,10)/6-311G*	6.50	6.50	8.34	8.54
MS-CASPT2	6.04	6.04	6.98	7.08

Table 2.1: The vertical excitations of MF, MF-w and MF-w dimer employing different active spaces and basis sets at the CASSCF and MS-CASPT2 levels in eV. Further, single point CASSCF and CASPT2 calculations of MF-w dimer without the water molecules are supplemented. They are denoted MF dimer. In the case of MF, the results are compared with the experiment in [33] and with the MS-CASPT2/SA-3-CAS(10,8)/6-31G* level in [19].

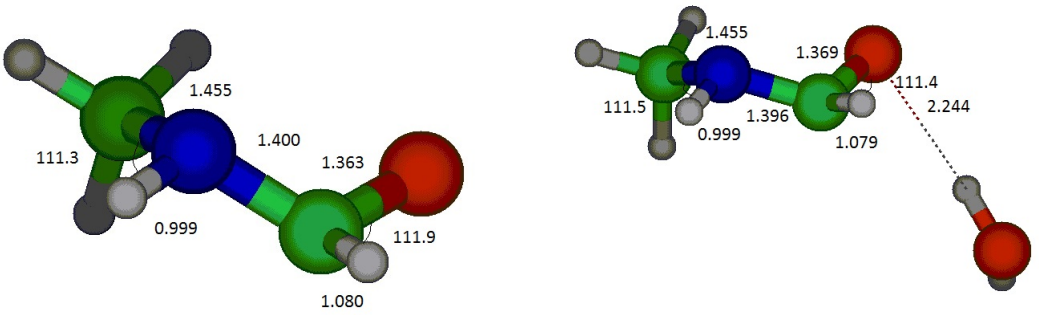

(a) S_1min of MF (b) S_1min of MF-w

Figure 2.7: The minimum of the first excited state of (a) MF and (b) MF-w monomers obtained at the SA-3-CASSCF(8,10)/6-31G* level. The distances are in Å and the angles in degrees.

and the geometrical parameters are given in Tables 2.2 and 2.3, respectively. The character of the conical intersection in both basis sets is $n \rightarrow \pi^*$. Besides, the excitation energy is delocalized regardless of the basis set. The geometry of CI is similar to the ground state and S_2min geometries. Note that the distance of CC atoms is the smallest in CI. This suggests that the system without the water molecules might "fall" into itself, form a dimer and relax into its ground state forming a new species.

The relative energies of all investigated points on the PES are summarized in Figure 2.8.

2.3.3 Non-Adiabatic Dynamics

The non-adiabatic dynamics ran for 100 trajectories starting from geometries obtained from the Wigner distribution. The first attempt of the dynamics of MF-w dimer failed because the MF molecules did not stack. Thus, the distance C(4)C(5) was frozen during the second attempt of the dynamics. 32 trajectories ran at least 450 fs from which 28 ran for 1000 fs. The rest of the trajectories ended due to convergence problems. Thus, they were removed from the final analysis.

Initial excitation energy was in the range 5.45-7.79 eV. At the beginning of the dynamics, the character of the excited state was delocalized in all 32 trajectories in agreement with the results in the vertical region (Table 2.1). The average $S_2 \rightarrow S_1$ hopping time was 35 fs. Only two trajectories relaxed into S_0 state, at the 17 and 31 fs. In the non-adiabatic dynamics of MF monomer in [19] which started on S_1 state, the lifetime was around 650 fs. The dynamics [19] examined the CN-cleavage

	E_1	$E(S2/S_1)$	E_2
MF	$n \rightarrow \pi^*$	-	$\pi \rightarrow \pi^*$
SA-3-CASSCF(4,5)/6-31G*	4.64	-	7.02
MS-CASPT2	4.52	-	6.67
SA-3-CASSCF(10,8)/6-31G* [19]	4.42	-	-
MS-CASPT2 [19]	4.46	-	-
MF-w	$n \rightarrow \pi^*$	-	$\pi \rightarrow \pi^*$
SA-3-CASSCF(4,5)/6-31G*	4.81	-	6.84
MS-CASPT2	4.77	-	6.53
MF-w dimer	$n \rightarrow \pi^*$	$n \rightarrow \pi^*$	$n \rightarrow \pi^*$
SA-3-CASSCF(8,10)/6-31G*	4.80	5.89	-
MS-CASPT2	4.99	5.85	-
Excitation	L	D	-
SA-3-CASSCF(8,10)/6-311G*	4.23	5.93	5.80
MS-CASPT2	4.82	5.87	5.72
Excitation	L	D	D

Table 2.2: The excited states minima of MF, MF-w monomers and MF-w dimer and CI of MF-w dimer. The energies are in eV.

	CO	CO	CC	H1	H2	OCNC	OCNC	OCCO
MF								
S_0 (a)	1.228	-	-	-	-	3.7	-	-
S_1min (b)	1.363	-	-	-	-	53.7	-	-
MF-w								
S_0 (a)	1.228	-	-	1.959	-	3.7	-	-
S_1min (b)	1.369	-	-	2.244	-	51.2	-	-
MF-w dimer								
Atoms	4,7	5,8	4,5	24,8	7,22	7,4,1,3	8,5,2,6	8,5,4,7
S_0 (a)	1.236	1.236	3.283	1.849	1.849	-2.7	2.7	-179.9
S_1min (a)	1.424	1.209	3.157	1.881	2.204	-59.8	3.1	-156.5
S_1min (b)	1.386	1.234	3.150	1.878	2.142	-57.1	4.1	-159.4
S_2min (a)	1.281	1.282	3.218	1.986	1.984	-22.3	21.7	-179.7
S_2/S_1 (a)	1.284	1.285	3.110	1.881	1.880	-19.8	19.8	180.0
S_2/S_1 (b)	1.287	1.287	3.116	1.886	1.883	-20.6	20.3	-179.9

Table 2.3: The geometry parameters of the excited state minima and of the crossing seam of MF, MF-w monomers, and MF-w dimer. The values are from optimizations obtained with the 6-311G* (symbolized (a)) and 6-31G* (symbolized (b)) basis sets. The distances are in Å, the angles in degrees. The numbers denote atoms of MF-w dimer as illustrated in Figure 2.6. The C-N bonds in the MF-w dimer structures do not change significantly. The distance was from the interval 1.335-1.379 Å.

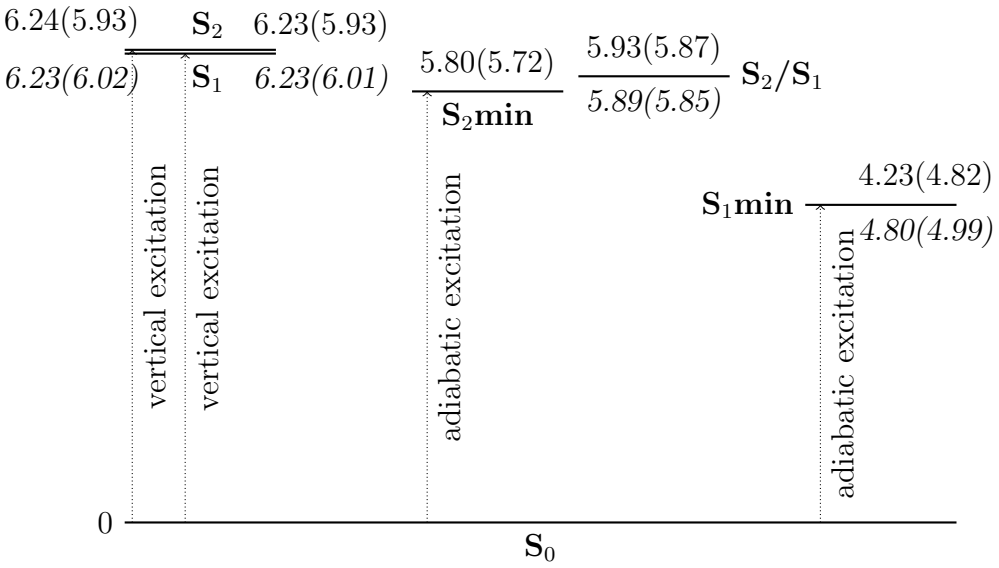

Figure 2.8: The energy diagram of MF-w dimer with the reference energy -568.231638 a.u. (-569.788851 a.u. for the MS-CASPT2 values) at the SA-3-CASSCF(8,10)/6-311G* level, and *slanted* with the reference energy -568.084140 a.u. (-569.514512 a.u. for the MS-CASPT2 values) at the SA-3-CASSCF(8,10)/6-31G* level.

relaxation with a bigger active space which included also $\pi \rightarrow \pi^*$ states. Since the goal of the present work was not to examine this relaxation channel, the results are not comparable.

During the dynamics simulations, the energy difference between S_2 and S_1 states for the 32 trajectories was monitored. A typical graph can be seen in Figure 2.9 which shows that at the beginning S_2 and S_1 states are almost degenerate. This degeneracy lasts until the system stays on PES of S_2. After the jump (in Figure 2.9 in 52.5 fs), the degeneracy is lifted quickly.

The geometries corresponding to the extremes of the energy difference curve and several geometries whose energy difference was around the average value of the trajectory were taken, as well as the geometries before and after the hop $S_2 \rightarrow S_1$ were investigated in more details. For these geometries, the localized or delocalized character of the excited state was determined. From this, the population of localized, partially delocalized and delocalized character of all 32 trajectories was calculated which is illustrated in Table 2.4. It can be seen that 40% of the all analyzed structures has the character partially delocalized, 39% delocalized, and only 21% localized.

In Figures 2.10a and 2.11a, the rhombi depict the evolution of the localiza-

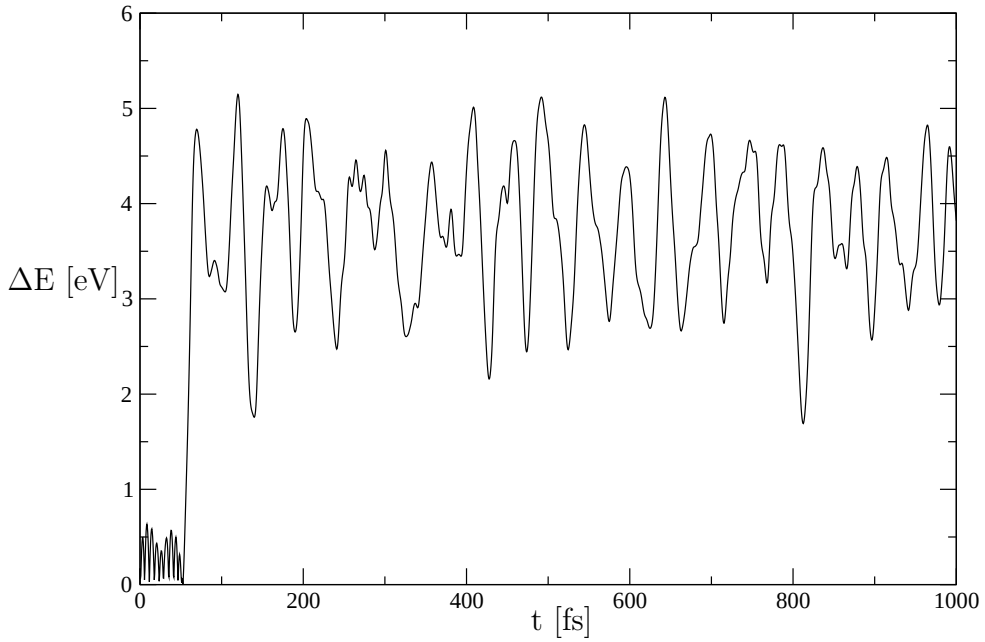

Figure 2.9: The energy difference of S_2 and S_1 states for one trajectory.

	fraction [%]
L	21
L/D	40
D	39

Table 2.4: The fraction of the localized, partially delocalized and delocalized excitation energy for 32 trajectories.

tion/delocalization in two typical trajectories. The system hopped to S_1 state at 114.0 fs and 22.5 fs in Figures 2.10a and 2.11a, respectively. Originally delocalized states start to partially localize after the hopping. For few points a complete delocalization was observed even after the hopping.

As it was pointed out in Section 1.5 that due to a small orbital overlap in the space and small value of transition dipole moments the excited states of $n \rightarrow \pi^*$ character are expected to be localized. Therefore a relatively large delocalization observed during the dynamics simulation is somehow surprising. In MF-w-dimer the bridging water molecules can affect the character of excited states and increase their extend of delocalization. This system is an example of donor-bridge-acceptor complex described in [57]. In such systems, both through-space electronic coupling (due to u_{short} and u_{Coupl}) and through-bond electronic coupling (via bridge molecules) can contribute to the total electronic coupling and the delocalization of the excited states. It has been shown by Lowe et al. [42] for the 1,4:5,8-bismethano-1,4,4a,5,8,8a-hexahydronaphthalene system that the coupling between two ethylene molecules can be enhanced by several orders of magnitude when the bridging alkane chain is present.

Therefore, the role of the water molecules was investigated by comparing of the character of excited states for the whole MF-w dimer complex and MF dimer after removing of water molecules. Typical results are shown in Figures 2.10a and 2.11a. The red squares indicate the character of states obtained for single point calculations MF dimer. The results show that the presence of the water molecules greatly influence the character of the excited state. In majority of the cases a decreased extend of delocalization was observed, indicating that the water increase the electronic coupling between the two chromophores. Note that for few cases the water molecules cause decreasing of the extend of delocalization.

In Subsection 2.3.2, the lengths of CO bonds or the OCNC torsions were suggested to determine the localization/delocalization of the excited state. Inspection of several points found during the dynamics simulations revealed that the former geometry parameter nicely reflects localized/delocalized character
of excited state of MF dimer. Thus, these were used to monitor this character during the whole course of dynamics. Figures 2.10b and 2.11b illustrates these lengths in

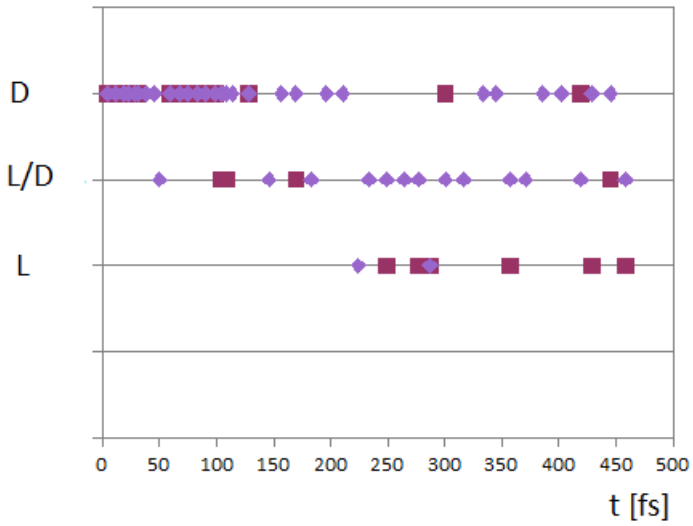

(a)

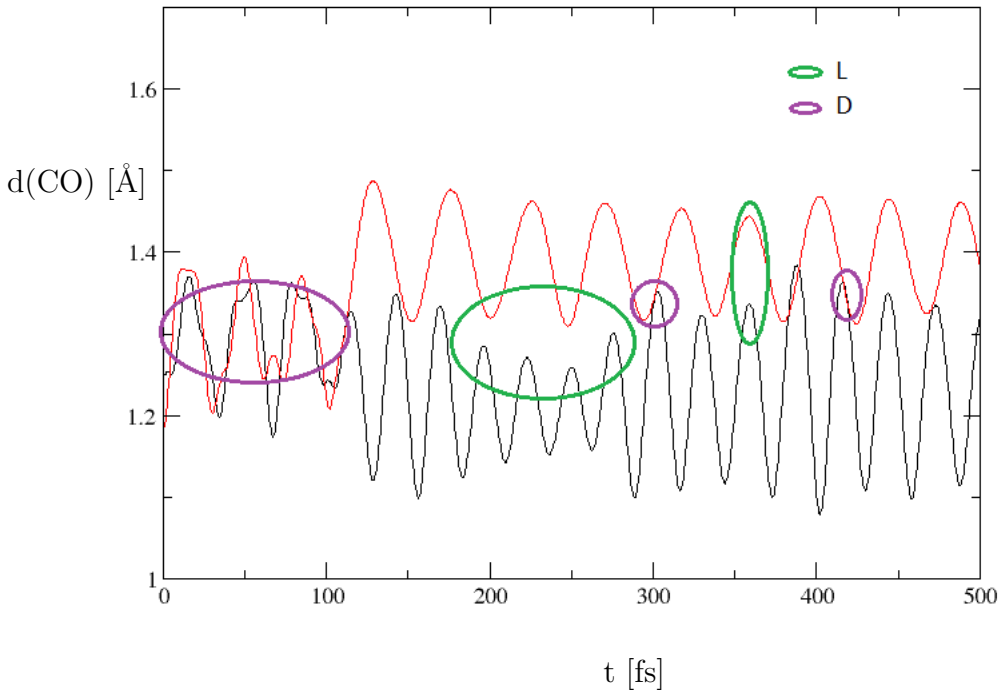

(b)

Figure 2.10: (a) The evolution of localization/delocalization during one trajectory. Rhombi depicts the character of MF-w dimer, square the single point calculations with the removed water molecules. (b) The evolution of CO bonds. The violet corresponds to delocalized character, the green to localized character.

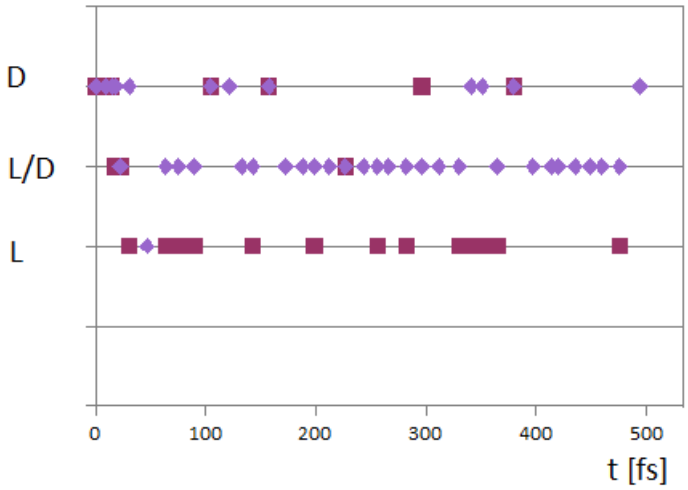

(a)

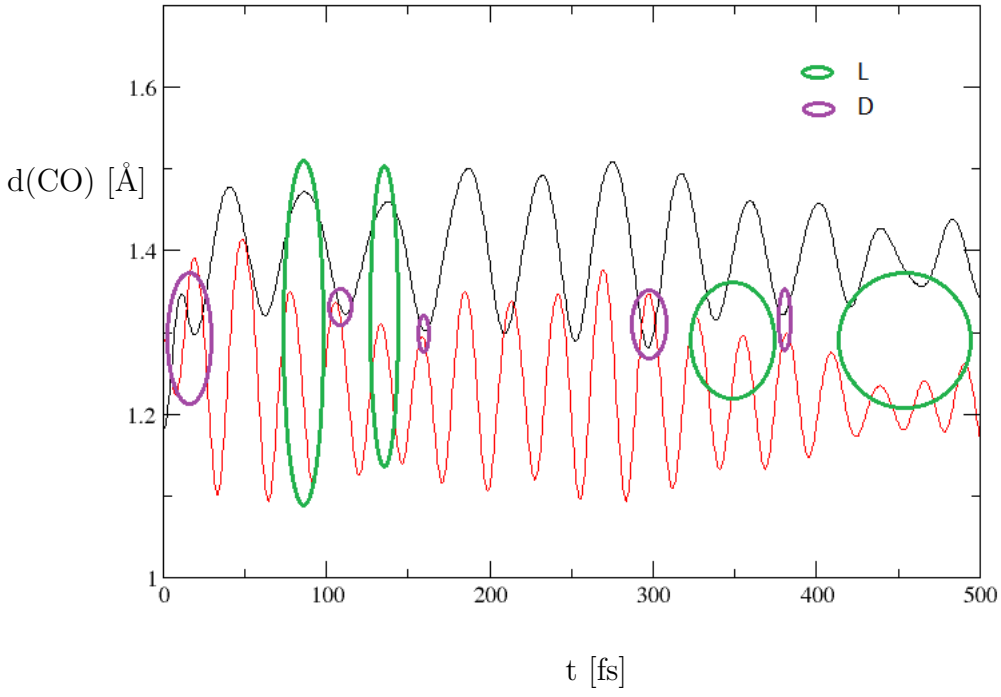

(b)

Figure 2.11: (a) The evolution of localization/delocalization during one trajectory. Rhombi depicts the character of MF-w dimer, square the single point calculations with the removed water molecules. (b) The evolution of CO bonds. The violet corresponds to delocalized character, the green to localized character.

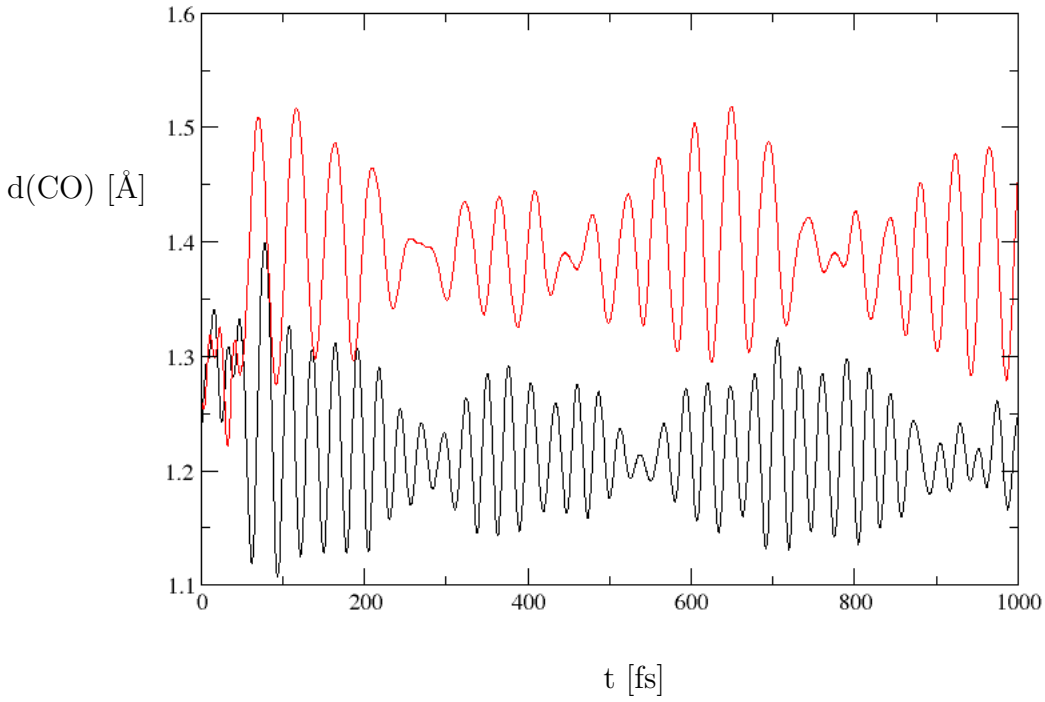

Figure 2.12: The evolution of the CO bonds on the both MF monomers during one typical trajectory.

the same two trajectories as in Figures 2.10a and 2.11a. The red curve represents the CO length on one MF, the black curve the CO length on the other one. At the beginning of both discussed dynamics, the CO bond lengths are very similar and the excited states are delocalized. Note that this feature was observed for all trajectories. The bond lengths oscillate around 1.3 Å, the value found for S_2min and S_2/S_1 conical intersection (see Table 2.3).

Figure 2.12 illustrates a typical behavior of CO bonds from 0 - 1000 fs. The delocalized character can be seen at the beginning where the CO bonds have almost equal length. After the fast hopping to S_1 state (at 52 fs in this particular trajectory), one CO bond starts to oscillate around the value of 1.4 Å, while the oscillation of the other CO bond is observed around 1.2 Å. Until 200 fs, the CO bonds meets several times. At these points, the excited state delocalized. After this time the excitation localizes although a partial delocalization is expected at some points in the region of 600 - 700 fs as the character of the CO bonds shows. The inspection of all trajectories reveals that MF dimer has preferably localized

character during the dynamics. This behavior was observed in 31 cases from 32 analyzed trajectories. In only a few cases there were more regions, where the CO curves cross indicating at least partial delocalization.

Conclusion

In the present work, electronically excited states of $n \rightarrow \pi^*$ character have been examined on the system composed of N-methylformamide dimer and two water molecules.

The potential energy surfaces have been described at the MCSCF level. The MS-CASPT2 method has been used to account for higher correlation effects. The excited state calculations were performed using the SA-CASSCF with different active spaces and the MS-CASPT2 method with the 6-31G* and 6-311G* basis sets. These calculations justify the use of the SA-3-CASSCF(8,10) level with the 6-31G* for the molecular dynamics simulations of the excited states of $n \rightarrow \pi^*$ character. S_2 and S_1 states both of $n \rightarrow \pi^*$ character have been found degenerate with the excitation energy of about 6 eV and delocalized character in the vertical region. The minimum of S_2 is delocalized with energy around 5.8 eV. The minimum of S_1, however, has localized character with the energy of about 4.99 eV. The only exception was found for the SA-3-CASSCF/6-311G*, where somehow a lower excitation energy (4.23 eV) was obtained. A conical intersection between S_2 and S_1 states has been found at the energy from 5.85 to 5.93 e V with the excitation delocalized. The geometries of S_2min and the conical intersection resulted in similar geometry to the ground state geometry: both N-methylformamides having almost a planar geometry. The localized S_1min had different geometries of the monomers. After comparing these results with the calculations of potential energy surfaces of N-methylformamide monomer and N-methylformamide dimer with and without the water molecules, CO bond and OCNC (or OCNH) torsion on the monomer were determined as the main indicators of localized character.

The non-adiabatic dynamics with the surface hopping algorithm has been calculated on this system. For all analyzed trajectories, the dynamics started in the

delocalized S_2 state and hopped into S_1 state after 35 fs on the average. The character of the excited state was examined and found to be mostly partially or fully delocalized.

Single point calculations of geometries obtained from the dynamics with the removed water molecules have been performed. The presence of the water molecules was found to strongly influence the localization/delocalization of the excitation and resulted in a decrease of the extend of delocalization in most cases. The analysis of geometrical parameters with respect to the character of the excited states showed that the localization/delocalization of excited N-methylformamide dimer can be studied by monitoring of CO bond lengths of both monomers. Based on this, a localized character of excited state was observed for majority of the population. The effect of water molecules on the photodynamics of interacting chromophores is an important issue related also to the photodynamics of nucleic acids where waters can directly bond to nucleobases [54, 55].

Appendix A

The Supplement Information to the HF theory

A.1 Slater Determinant

The Slater determinant is an antisymmetric wavefunction written in a determinant form:

$$\Psi(\boldsymbol{x_1}, \boldsymbol{x_2}, ..., \boldsymbol{x_N}) = \frac{1}{\sqrt{N!}} \begin{vmatrix} \chi_i(\boldsymbol{x_1}) & \chi_j(\boldsymbol{x_1}) & \cdots & \chi_k(\boldsymbol{x_1}) \\ \chi_i(\boldsymbol{x_2}) & \chi_j(\boldsymbol{x_2}) & \cdots & \chi_k(\boldsymbol{x_2}) \\ \vdots & \vdots & \ddots & \vdots \\ \chi_i(\boldsymbol{x_N}) & \chi_j(\boldsymbol{x_N}) & \cdots & \chi_k(\boldsymbol{x_N}) \end{vmatrix} \tag{A.1.1}$$

In (A.1.1) is the general form of Slater determinant for N electrons which occupy N spin orbitals $\chi_i(\boldsymbol{x_j})$. The spin orbitals constitute an orthonormal basis set $\langle\chi_i|\chi_j\rangle = \delta_{ij}$, and their coordinates $\boldsymbol{x_j}$ represent the spatial coordinates $\boldsymbol{r}$ and the spin of electrons ($\alpha(\omega)$ the spin up, $\beta(\omega)$ the spin down)

$$\chi(\boldsymbol{x}) = \begin{cases} \psi(\boldsymbol{r})\alpha(\omega) \\ or \\ \psi(\boldsymbol{r})\beta(\omega) \end{cases}$$

The Slater determinant can be simplified to the form

$$|\Psi_0\rangle = |\chi_1\chi_2\cdots\chi_k\rangle \tag{A.1.2}$$

where only the diagonal terms of (A.1.1) are written.

A.2 Configuration State Function

Exact solutions of Equation (1.0.2) are eigenfunctions of $\hat{H}$, $\hat{S}_z$ and $\hat{S}^2$ if $\hat{H}$ does not contain any spin coordinates. This is fulfilled in the nonrelativistic approach. A Slater determinant is an approximation to the solution of the Schrödinger equation (1.0.2) and, therefore, does not have to be a pure spin state (singlet, doublet, triplet, etc.). However, Slater determinants can be constrained to be eigenfunctions of $\hat{S}_z$. This does not entail that they also are eigenfunctions of $\hat{S}^2$. One can obtain eigenfunctions of $\hat{S}^2$ by a linear combination of Slater determinants. These functions are called Spin-Adapted Configurations or Configuration State Functions (CSF).

A.3 Fock Operator

In the HF method, a Slater determinant is formed from spin orbitals obtained from the HF equation (1.2.3). The Fock operator (1.2.2) can be rewritten to the form

$$\hat{f}(i) = \hat{h}(i) + \sum_b [\mathcal{J}_b(i) - \mathcal{K}_b(i)] \tag{A.3.1}$$

in which the one-electron operator $\hat{h}(i)$

$$\hat{h}(i) = -\frac{1}{2}\Delta_i - \sum_{A=1}^{M} \frac{Z_A}{r_{iA}} \tag{A.3.2}$$

is the sum of the kinetic energy of the i-th electron and the potential energy for the attraction of the same electron to the nuclei, and the rest of the Fock operator represents the HF potential of the i-th electron

$$\hat{v}^{HF}(i) = \sum_b [\hat{\mathcal{J}}_b(i) - \hat{\mathcal{K}}_b(i)] \tag{A.3.3}$$

where $\hat{\mathcal{J}}_b(i)$ is the coulomb operator representing a one-electron repulsive potential which the i-th electron experiences, and $\hat{\mathcal{K}}_b(i)$ is the exchange operator which is a result of fermionic nature of electrons. The one-electron potential, the coulomb operator, is an averaged field defined as

$$\hat{\mathcal{J}}_b(i)\chi_a(i) = [\int \chi_b^*(j) r_{ij}^{-1} \chi_b(j) dx_j]\chi_a(i) \tag{A.3.4}$$

and the exchange operator is defined as

$$\hat{\mathcal{K}}_b(i)\chi_a(i) = [\int \chi_b^*(j) r_{ij}^{-1} \chi_a(j) dx_j]\chi_b(i) \tag{A.3.5}$$

From (A.3.4) and (A.3.5), it can be seen that $\hat{v}^H F(i)$ depends on the spin orbitals; therefore, an initial guess is done in the HF equation (1.2.3); the newly obtained spin orbitals are then used in obtaining new $\hat{\mathcal{J}}_b(i)$ and $\hat{\mathcal{K}}_b(i)$. The HF equation can be solved again with the new Fock operator. This repeats until the spin orbitals do not change significantly with obtaining a new Fock operator. The procedure is called the Size-Consistent Field (SCF) method.

A.4 Basis Set

Section 1.2 introduced the LCAO method, where the usage of functions of atomic orbitals was suggested. Indeed, atomic orbitals localized on nuclei describe electrons in the vicinity of nuclei properly while the bond region is well described by their linear combination. However, it is not necessary to use only the atomic orbitals. The idea is to find functions that are similar to the atomic orbitals.

The ϕ_μ can be written as a product of an angle part $Y(\theta, \varphi)$ and a radial part $R(r)$. Normally, quantum chemistry calculates with a real Hamiltonian; thus the wavefunctions and their parts are also real.

There are two types of radial functions commonly used:

1. Slater-type function (relation (A.4.1))

$$R^{SF} = \left(\frac{(2\zeta)^n}{(2n)!}\right)^{\frac{1}{2}} r^{n-1} exp(-\zeta r) \tag{A.4.1}$$

2. Gaussian-type function (relation (A.4.2))

$$R^{GF} = C(l, \alpha) r^l exp(-\alpha(r - r_A)^2) \tag{A.4.2}$$

In equation (A.4.1), n indicates the main quantum number, and ζ indicates the Slater orbital exponent. In equation (A.4.2), l is the orbital quantum number, $C(l, \alpha)$ is the normalization factor dependent on l and α, α is the Gaussian orbital exponent and, finally, r_A indicates that the function is centered on nucleus A.

The Slater-type function approximates atomic orbitals better than the Gaussian-type; however, four-centered two-electron integrals are calculated during the SCF procedure, which is very difficult. The usage of the
Gaussian-type functions reduces the four-centered integrals to two-centered integrals. Therefore Gaussian-type basis functions are widely preferred.

There is also a possibility to approximate a Slater-type function by an expansion of Gaussian-type functions

$$R^{CGF}(r - R_A) = \sum_{p=1}^{L} d_{p\mu} R_p^{GF}(\alpha_{p\mu}, r - R_A) \tag{A.4.3}$$

which is called contracted Gaussian function (CGF); $d_{p\mu}$ indicates a contraction coefficient.

Many types of basis were developed. For this present work, the 6-31G* and 6-311G* basis sets are relevant. The marking 6-31G indicates that the inner shell functions are contractions of six Gaussian-type functions, while the valence basis functions are described by a contraction of three Gaussian-type functions, and one Gaussian-type function. The star in the 6-31G* entails that polarization functions are included, namely six uncontracted Cartesian-Gaussian-d-type functions. The term Cartesian-Gaussian means that here the d-functions are linear combinations of usual five d-functions and one s-type function.

The 6-311G* basis set differs from the 6-31G* only by the description of the valence shell. Here, it is a contraction of three Gaussian-type functions, and two Gaussian-type functions.

Bibliography

[1] ABO-RIZIQ, A. - GRACE, L. - NIR, E. - KABELAC, M. - HOBZA, P. - de VRIES, M. S.: Photochemical selectivity in guanine-cytosine base-pair structures. In *Proceedings of the National Academy of Sciences*, 2005, vol. 102, no. 1, pp. 20-23.

[2] BARBATTI, M. - AQUINO, A. J. A. - LISCHKA, H.: The UV absorption of nucleobases: Semi-classical ab initio spectra simulations. In *Physical Chemistry Chemical Physics*, 2010, vol. 12, no. 19, pp. 4959-4967.

[3] BARBATTI, M. - AQUINO, A. J. A. - SZYMCZAK, J. J. - NACHTIGALLOVÁ, D. - HOBZA, P. - LISCHKA, H.: Relaxation mechanisms of UV-photoexcited DNA and RNA nucleobases. In *Proceedings of the National Academy of Sciences*, 2010, vol. 107, no. 50, pp. 21453-21458.

[4] BARBATTI, M. - AQUINO, A. J. A. - SZYMCZAK, J. J. - NACHTIGALLOVÁ, D. - LISCHKA, H.: Photodynamical simulations of cytosine: Characterization of the ultrafast bi-exponential UV deactivation. In *Physical Chemistry Chemical Physics*, 2011, vol. 13, no. 13, pp. 6145-6155.

[5] BARBATTI, M. - GRANUCCI, G. - PERSICO, M. - RUCKENBAUER, M. - VAZDAR, M. - ECKERT-MAKSIC, M. - LISCHKA, H.: The on-the-fly surface-hopping program system NEWTON-X: Application to ab initio simulation of the nonadiabatic photodynamics of benchmark systems. In *Journal of Photochemistry and Photobiology A-Chemistry*, 2007, vol. 190, no. 2-3, pp. 228-240.

[6] M. Barbatti, G. Granucci, M. Ruckenbauer, J. Pittner, M. Persico, H. Lischka, NEWTON-X: a package for Newtonian dynamics close to the crossing seam, version 1.2, www.newtonx.org (2010).

[7] BARBATTI, M. - SHEPARD, R. - LISCHKA, H.: *Computational and Methodological Elements of Nonadiabatic Trajectory Dynamics Simulations of Molecules, in Conical Intersections: Theory, Computation and Experiment.* W. Domcke, D. R. Yarkony, and H. Köppel, Eds. Singapore: World Scientific, 2010. pp. 2-18.

[8] BESLEY, N. A. - HIRST, J. D.: Ab inition study of the electronic spectrum of formamide with explicit solvent. In *Journal of the American Chemical Society*, 1999, vol. 121, no. 37, pp. 8559-8566.

[9] BLANCAFORT, L. - COHEN, B. - HARE, P. M. - KOHLER, B. - ROBB, M. A.: Singlet excited-state dynamics of 5-fluorocytosine and cytosine: An experimental and computational study. In *Journal of Physical Chemistry A*, 2005, vol. 109, no. 20, pp. 4431-4436.

[10] BOUVIER, B. - GUSTAVSSON, T. - MARKOVITSI, D. - MILLIÉ, P.: Dipolar coupling between electronic transitions of the DNA bases and its relevance to exciton states in double helices. In *Chemical Physics*, 2002, vol. 275, no. 1-3, pp. 75-92.

[11] BUCHVAROV, I. - WANG, Q. - RAYTCHEV, M. - TRIFINOV, A. - FIEBIG, T.: Electronic energy delocalization and dissipation in single- and double-stranded DNA. In *Proceedings of the National Academy of Sciences*, 2007, vol. 104, no. 12, pp. 4794-4797.

[12] CADET, J. - MOURET, S. - RAVANAT, J. L. - DOUKI, T.: Photoinduced damage to cellular DNA: Direct and photosensitized reactions. In *Photochemistry and Photobiology*, 2012, vol. 88, no. 5, pp. 1048-1065.

[13] CANUEL, C. - MONS, M. - PIUZZI, F. - TARDIVEL, B. - DIMICOLI, I. - ELHANINE, M.: Excited states dynamics of DNA and RNA bases: Characterization of a stepwise deactivation pathway in the gas phase. In *Journal of Chemical Physics*, 2005, vol. 122, no. 7, 074316.

[14] Columbus, H. Lischka, R. Shepard, I. Shavitt, R. M. Pitzer, M. Dallos, Th. Müller, P. G. Szalay, F. B. Brown, R. Ahlrichs, H. J. Böhm, A. Chang, D. C. Comeau, R. Gdanitz, H. Dachsel, C. Ehrhardt, M. Ernzerhof, P. Höchtl, S. Irle, G. Kedziora, T. Kovar, V. Parasuk, M. J. M. Pepper, P. Scharf, H. Schiffer, M. Schindler, M. Schüler, M. Seth, E. A. Stahlberg, J.-G. Zhao, S. Yabushita, Z. Zhang, M. Barbatti, S. Matsika, M. Schuurmann, D. R. Yarkony, S. R. Brozell, E. V. Beck, and J.-P. Blaudeau, M. Ruckenbauer, B. Sellner, F. Plasser, and J. J. Szymczak, COLUMBUS, an ab initio electronic structure program, release 7.0 (2012).

R. Shepard Int. J. Quant. Chem. 1987, XXXI, 33.

R. Shepard, in: Modern Electronic Structure Theory Part I, ed. D. R. Yarkony, (World Scientific, Singapore), 1995, p. 345.

[15] CRESPO-HERNÁNDEZ, C. E. - COHEN, B. - HARE, P. M. - KOHLER, B.: Ultrafast excited-state dynamics in nucleic acids. In *Chemical Reviews*, 2004, vol. 104, no. 4, pp. 1977-2019.

[16] CRESPO-HERNÁNDEZ, C. E. - COHEN, B. - KOHLER, B.: Base stacking controls excited-state dynamics in A·T DNA. In *Nature*, 2005, vol. 436, no. 11188, pp. 1141-1144.

[17] CRESPO-HERNÁNDEZ, C. E. - KOHLER, B.: Influence of secondary structure on electronic energy relaxation in adenine homopolymers. In *Journal of Physical Chemistry B*, 2004, vol. 108, no. 30, pp. 11182-11188.

[18] CRESPO-HERNÁNDEZ, C. E. - de La Harpe, K. - KOHLER, B.: Ground-state recovery following UV excitation is much slower in G·C-DNA duplexes and hairpins than in mononucleotides. In *Journal of the American Chemical Society*, 2008, vol. 130, no. 33, 10844.

[19] CRESPO-OTERO, R. - MARDYUKOV, A. - SANCHEZ-GARCIA, E. - BARBATTI, M. - SANDER, W. 2013. Photochemistry of N-methylformamide: Matrix isolation and nonadiabatic dynamics. In *ChemPhysChem*, 2013, vol. 14, no. 4, pp. 827-836.

[20] DAVYDOV, A. S.: *Theory of Molecular Excitons.* New York: McGraw-Hill, 1971.

[21] DEGLMANN, P. - MAY, K. - FURCHE, F. - AHLRICHS, R.: Nuclear second analytical derivative calculations using auxiliary basis set expansion. In *Chemical Physics Letters*, 2004, vol. 384, no. 1-3, pp. 103-107.

[22] EAST, A. L. L. - LIM, E. C.: Naphtalene dimer: Electronic states, excimers, and triplet decay. In *Journal of Chemical Physics*, 2000, vol. 113, no. 20, pp. 8981-8994.

[23] EICHKOM, K. - WEIGEND, O. - TREUTLER, O. - AHLIRCHS, R.: Auxiliary basis sets for main row atoms and transition metals and their use to approximate Coulomb potentials. In *Theoretical Chemistry Accounts*, 1997, vol. 97, no. 1-4, pp. 119-124.

[24] FINLEY, J. - MALMQVIST, P. Å. - ROOS, B. O. - SERRANO-ANDRÉS, L.: The multi-state CASPT2 method. In *Chemical Physics Letters*, 1998, vol. 288, no. 2-4, pp. 299-306.

[25] FRENKEL, J.: On the transformation of light into heat in solids. II. In *Physical Review*, 1931, vol. 37, 1276.

[26] Gaussian 09, Revision D.01, M. J. Frisch, G. W. Trucks, H. B. Schlegel, G. E. Scuseria, M. A. Robb, J. R. Cheeseman, G. Scalmani, V. Barone, B. Mennucci, G. A. Petersson, H. Nakatsuji, M. Caricato, X. Li, H. P. Hratchian, A. F. Izmaylov, J. Bloino, G. Zheng, J. L. Sonnenberg, M. Hada, M. Ehara, K. Toyota, R. Fukuda, J. Hasegawa, M. Ishida, T. Nakajima, Y. Honda, O. Kitao, H. Nakai, T. Vreven, J. A. Montgomery, Jr., J. E. Peralta, F. Ogliaro, M. Bearpark, J. J. Heyd, E. Brothers, K. N. Kudin, V. N. Staroverov, T. Keith, R. Kobayashi, J. Normand, K. Raghavachari, A. Rendell, J. C. Burant, S. S. Iyengar, J. Tomasi, M. Cossi, N. Rega, J. M. Millam, M. Klene, J. E. Knox, J. B. Cross, V. Bakken, C. Adamo, J. Jaramillo, R. Gomperts, R. E. Stratmann, O. Yazyev, A. J. Austin, R. Cammi, C. Pomelli, J. W. Ochterski, R. L. Martin, K. Morokuma, V. G. Zakrzewski, G. A. Voth, P. Salvador, J. J. Dannenberg, S.

Dapprich, A. D. Daniels, O. Farkas, J. B. Foresman, J. V. Ortiz, J. Cioslowski, and D. J. Fox, Gaussian, Inc., Wallingford CT, 2013.

[27] GHIGO, G. - ROOS, B. O. - MALMQVIST, P. Å.: A modified definition of the zeroth-order Hamiltonian in multiconfigurational perturbation theory (CASPT2). In *Chemical Physics Letters*, 2004, vol. 396, no. 1-3, pp. 142-149.

[28] GOODSHELL, D. S.: The molecular perspective: Ultraviolet light and pyrimidine dimers. In *The Oncologist Fundamentals of Cancer Medicine*, 2001, vol. 6, pp. 298-299.

[29] HARIHARAN, P. C. - POPLE, J. A.: Influence of polarization functions on molecular-orbital hydrogenation energies. In *Theoreitca Chimica Acta*, 1973, vol. 28, no. 3, pp. 213-222.

[30] HEHRE, W. J. - DITCHFIELD, R. - POPLE, J. A.: Self-consistent molecular-orbital methods. 12. Further extensions of Gaussian-type basis sets for use in molecular-orbital studies of organic-molecules. In *Journal of Chemical Physics*, 1972, vol. 56, no. 5, p. 2257.

[31] JUNGWIRTH, P. *Klasická a kvantová molekulová dynamika.* unpublished work.

[32] KARLSTRÖM, R. - LINDH, R. - MALMQVIST, P.- Å. - ROOS, B. O. - RYDE, U. - VERYAZOV, V. - WIDMARK, P. O. - COSSI, B. - SCHIMMELPFENNIG, P. - NEOGRADY, P.: MOLCAS: a program package for computational chemistry. In *Computational Materials Science*, 2003, vol. 28, no. 2, pp. 222-239.

[33] KAYA, K. - NAGAKURA, S.: Vacuum ultraviolet absorption spectra of simple amides. In *Theoretica Chimica Acta*, 1967, vol. 7, no. 2, 117.

[34] KISTLER, K. A. - SPANO, F. C. - MATSIKA, S.: A benchmark of excitonic couplings derived from atomic transition charges. In *Journal of Physical Chemistry B*, 2013, vol. 117, no. 7, pp. 2032-2044.

[35] KLESSINGER, M. - MICHL, J.: *Excited states and photochemistry of organic molecules.* New York: VCH Publishers, Inc., 1995, p. 185.

[36] KRAUSS, M. - WEBB, S. P.: Solvation and the excited states of formamide. In *Journal of Chemical Physics*, 1997, vol. 107, no. 15, pp. 5771-5775.

[37] KRISHNAN, R.- BINKLEY, J. S. - SEEGER, R. - POPLE, J. A.: Self-consistent molecular orbital methods. 20. basis set for correlated wave-functions. In *Journal of Chemical Physics*, 1980, vol. 1, pp. 650-654.

[38] KUNDU, L. M. - LINNE, U. - MARAHIEL, M. - CARELL, T.: RNA is more UV resistant than DNA: the formation of UV-induced DNA lesions is strongly sequence and conformation dependent. In *Chemistry- A European Journal*, 2004, vol. 10, no. 22, pp. 5697-5705.

[39] KWOK, W. M. - MA, C. S. - PHILLIPS, D. L.: Femtosecond time- and wavelength-resolved fluorescence and absorption spectroscopic study of the excited states of adenosine and an adenine oligomer. In *Journal of the American Chemical Society*, 2006, vol. 128, no. 36, pp. 11894-11905.

[40] LISCHKA, H. - SHEPARD, R. - BROWN, F. B. - SHAVITT, I.: New implementation of the graphical unitary-group approach for multi-reference direct configuration-interaction calculations. In *International Journal of Quantum Chemistry*, 1981, vol. 15, pp. 91-100.

[41] LISCHKA, H. - SHEPARD, R. - PITZER, R. M. - SHAVITT, I. - DALLOS, M. - MÜLLER, Th. - SZALAY, P. G. - SETH, M. - KEDZIORA, G. S. - YABUSHITA, S. - ZHANG, Z.: High-level multireference methods in the quantum-chemistry program system COLUMBUS: Analytic MR-CISD and MR-AQCC gradients and MR-AQCC-LRT for excited states, GUGA spin-orbit CI and parallel CI density. In *Physical Chemistry Chemical Physics*, 2001, vol. 3, no. 5, pp. 664-673.

[42] LOVE, D. E. - Nachtigallová, D. - JORDAN, K. D. - LAWSON, J. M. - PADDON-ROW, M. N.: Electronically excited states of 1,4:5,8-bismethano-1,4,4a,5,8,8a-hexahydronaphtalene, a nonconjugated diene: Comparison of theory and experiment. In *Journal of the American Chemical Society*, 1996, vol. 118, no. 6, pp. 1235-1240.

[43] MARKOVITSI, D. - GUSTAVSSON, T. - SHARONOV, A.: Cooperative effects in the photophysical properties of self-associated triguanosine diphosphates. In *Photochemistry and Photobiology*, 2004, vol. 79, no. 6, pp. 526-530.

[44] McLEAN, D. - CHANDLER, G. S.: Contracted Gaussian-basis sets for molecular calculations. 1. 2nd row atoms, Z=11-18. In *Journal of Chemical Physics*, 1980, vol. 72, no. 10., pp. 5639-5648.

[45] MIDDLETON, C. T. - de La HARPE, K. - SU, C. - LAW, Y. K. - CRESPO-HERNÁNDEZ, C. E. - KOHLER, B.: DNA excited-state dynamics: From single bases to the double helix. In *Annual Review of Physical Chemistry*, 2009, vol. 60, pp. 217-239.

[46] Molcas 7.4: F. Aquilante, L. De Vico, N. Ferré, G. Ghigo, P.-Å. Malmqvist, P. Neogrády, T.B. Pedersen, M. Pitonak, M. Reiher, B.O. Roos, L. Serrano-Andrés, M. Urban, V. Veryazov, R. Lindh, Journal of Computational Chemistry, 31, 224, 2010.

[47] NACHTIGALLOVÁ, D. - HOBZA, P. - RITZE, H.: Electronic splitting in the excited states of DNA base homodimers and -trimers: An evaluation of short-range and Coulombic interactions. In *Physical Chemistry Chemical Physics*, 2008, vol. 10, no. 37, pp. 5689-5697.

[48] NACHTIGALLOVÁ, D. - ZELENÝ, T. - RUCKENBAUER, M. - MÜLLER, T. - BARBATTI, M. - HOBZA, P. - LISCHKA, H.: Does stacking restrain the photodynamics of individual nucleobases?. In *Journal of the American Chemical Society*, 2010, vol. 132, no. 24, 8261.

[49] PLASSER, F. - AQUINO, A. J. A. - LISCHKA, H. - NACHTIGALLOVÁ, D.: Electronic excitation processes in single-strand and double-strand DNA: A computational approach. In *Topics in Current Chemistry*, 2014, vol. , no. .

[50] PLASSER, F. - LISCHKA, H.: Electronic excitation and structural relaxation of the adenine dinucleotide in gas phase and solution. In *Photochemical and Photobiological Sciences*, 2013, vol. 12, no. 8, pp. 1440-1452.

[51] PLESSOW, R. - BROCKHINKE, A. - EIMER, W. - KOHSE-HÖINGHAUS, K.: Intrinsic time- and wavelength-resolved fluorescence of oligonucleotides: A systematic investigation using a novel picosecond laser approach. *Journal of Physical Chemistry B*, 2000, vol. 104, no. 15, pp. 3695-3704.

[52] RITZE, H. - HOBZA, P. - NACHTIGALLOVÁ, D.: Electronic coupling in the excited electronic state of stacked DNA base homodimers. In *Physical Chemistry Chemical Physics*, 2007, vol. 9, no. 14, pp. 1672-1675.

[53] ROOS, B. O., ed.: *Lecture Notes in Quantum Chemistry: European Summer School in Quantum Chemistry.* Berlin: Springer-Verlag, 1992. pp. 154-252, 333-336.

[54] SCHNEIDER, B. - BERMAN, H. M.: Hydration of the DNA bases is local. In *Biophysical Journal*, 1995, vol. 69, no. 6, pp. 2661-2669.

[55] SCHNEIDER, B. - COHEN, D. M. - SCHLEIFER, L. SRINIVASAN, A. R. - OLSON, W. K. - BERMAN, H. M.: A systematic method for studying the spatial distribution of water molecules around nucleic acid bases. In *Biophysical Journal*, 1993, vol. 65, no. 6, pp. 2291-3203.

[56] SCHOLES, G. D. - GHIGGINO, K. P.: Electronic interactions and interchromophore excitation transfer. In *Journal of Physical Chemistry*, 1994, vol. 98, no. 17, pp. 4580-4590.

[57] SCHOLES, G. D. - GHIGGINO, K. P.: Mechanisms of excitation transfer in multichromophoric systems. In *Journal of Photochemistry and Photobiology A-Chemistry*, 1994, vol. 80, no. 1-3, pp. 355-362.

[58] SHEPARD, R. - LISCHKA, H. - SZALAY, P. G. - KOVAR, T. - ERNZERHOF, M.: A general multireference configuration-interaction gradient program. In *Journal of Chemical Physics*, 1992, vol. 96, no. 3, pp. 2085-2098.

[59] SHEPARD, R. - SHAVITT, I. - PITZER, R. M. - COMEAU, D. C. - PEPPER, M. - LISCHKA, H. - SZALAY, P. G. - AHLRICHS, R. - BROWN, F. B. - ZHAO, J.: A progress report on the status of the Columbus MRCI program system. In *International Journal of Quantum Chemistry*, 1988, vol. 22, pp. 149-165.

[60] SHIN, S.- KURAWAKI, A. - HAMADA, Y. - SHINYA, K. - OHNO, K. - TOHARA, A. - SATO, M.: Conformational behavior of N-methylformamide in the gas, matrix, and solution states as revealed by IR and NMR spectroscopic measurements and by theoretical calculations. In *Journal of Molecular Structures*, 2006, vol. 791, no. 1-3, pp. 30-40.

[61] SKÁLA, L.: *Kvantová teorie molekul.* Praha: Karolinum, 1995, s. 61-67.

[62] SOBOLEWSKI, A. L.: Ab initio study of the potential energy functions relevant for hydrogen transfer in formamide, its dimer and its complex with water. In *Journal of Photochemistry and Photobiology A: Chemistry*, 1995, vol. 89, no. 2, pp. 89-97.

[63] SZABO, A. - OSTLUND, N. S.: *Modern Quantum Chemistry: Introduction to Advanced Electronic Structure Theory.* 2nd ed. Mineola, New York: Dover Publications, Inc., 1996, pp. 39-229.

[64] SZYMCZAK, J. J. - BARBATTI, M. - HOO, J. T. S. - ADKINS, J. A. - WINDUS, T. L. - NACHTIGALLOVÁ, D. - LISCHKA, H.: Photodynamics simulations of thymine: Relaxation into the first excited singlet state. In *Journal of Physical Chemistry A*, 2009, vol. 113, no. 45, pp. 12686-12693.

[65] TREUTLER, O. - AHLRICHS, R.: Efficient molecular numerical integration schemes. In *Journal of Chemical Physics*, 1995, vol. 102, no. 1, pp. 346-354.

[66] TROGANIS, A. N. - SICILIA, L. - BARBAROSSOU, K. - GEROTHANASSIS, I. P. - RUSSO, N.: Solvation properties of N-substituted cis and trans ammides are not identical: Significant enthalpy and entropy changes are revealed by the use off variable temperature H-1 NMR in aqueous and chloroform solutions and ab initio calculations. In *Journal of Physical Chemistry A*, 2005, vol. 109, no. 51, pp. 11878-11884.

[67] TULLY, J. C.: Molecular-dynamics with electronic-transitions. In *Journal of Chemical Physics*, 1990, vol. 93, no. 2, pp. 1061-1071.

[68] ULLRICH, S. - SCHULTZ, T. - ZGIERSKI, M. Z. - STOLLOW, A.: Electronic relaxation dynamics in DNA and RNA bases studied by time-resolved photo-

electron spectroscopy. In *Physical Chemistry Chemical Physics*, 2004, vol. 6, no. 10, pp. 2796-2894.

[69] VAYA, I. - MIANNAY, F. A. - GUSTAVSSON, T. - MARKOVITSI, D.: High-energy long-lived excited states in DNA double strands. In *ChemPhysChem*, 2010, vol. 11, no. 5, pp. 987-989.

[70] VERYAZOV, V. - WIDMARK, P.-O. - SERRANO-ANDRES, L. - LINDH, R. - ROOS, B. O.: 2MOLCAS as a development platform for quantum chemistry software. In *International Journal of Quantum Chemistry*, 2004, vol. 100, no. 4, pp. 626-635.

[71] WEIGEND, F.: A fully direct RI-HF algorithm: Implementation, optimised auxiliary basis sets, demonstration of accuracy and efficiency. In *Physical Chemistry Chemical Physics*, 2002, vol. 4, no. 18, pp. 4285-4291.